

# Selective regulation of clathrin-mediated epidermal growth factor receptor signaling and endocytosis by phospholipase C and calcium

Ralph Christian Delos Santos<sup>a</sup>, Stephen Bautista<sup>a</sup>, Stefanie Lucarelli<sup>a</sup>, Leslie N. Bone<sup>a</sup>, Roy M. Dayam<sup>a</sup>, John Abousawan<sup>a</sup>, Roberto J. Botelho<sup>a</sup>, and Costin N. Antonescu<sup>a,b,\*</sup>

<sup>a</sup>Department of Chemistry and Biology and Graduate Program in Molecular Science, Ryerson University, Toronto, ON M5B 2K3, Canada; <sup>b</sup>Keenan Research Centre for Biomedical Science of St. Michael's Hospital, Toronto, ON M5B 1W8, Canada

**ABSTRACT** Clathrin-mediated endocytosis is a major regulator of cell-surface protein internalization. Clathrin and other proteins assemble into small invaginating structures at the plasma membrane termed clathrin-coated pits (CCPs) that mediate vesicle formation. In addition, epidermal growth factor receptor (EGFR) signaling is regulated by its accumulation within CCPs. Given the diversity of proteins regulated by clathrin-mediated endocytosis, how this process may distinctly regulate specific receptors is a key question. We examined the selective regulation of clathrin-dependent EGFR signaling and endocytosis. We find that perturbations of phospholipase C $\gamma$ 1 (PLC $\gamma$ 1), Ca<sup>2+</sup>, or protein kinase C (PKC) impair clathrin-mediated endocytosis of EGFR, the formation of CCPs harboring EGFR, and EGFR signaling. Each of these manipulations was without effect on the clathrin-mediated endocytosis of transferrin receptor (TfR). EGFR and TfR were recruited to largely distinct clathrin structures. In addition to control of initiation and assembly of CCPs, EGF stimulation also elicited a Ca<sup>2+</sup>- and PKC-dependent reduction in synaptojanin1 recruitment to clathrin structures, indicating broad control of CCP assembly by Ca<sup>2+</sup> signals. Hence EGFR elicits PLC $\gamma$ 1-calcium signals to facilitate formation of a subset of CCPs, thus modulating its own signaling and endocytosis. This provides evidence for the versatility of CCPs to control diverse cellular processes.

**Monitoring Editor**  
Jean E. Gruenberg  
University of Geneva

Received: Dec 22, 2016  
Revised: Jul 10, 2017  
Accepted: Aug 9, 2017

This article was published online ahead of print in MBoC in Press (<http://www.molbiolcell.org/cgi/doi/10.1091/mbc.E16-12-0871>) on August 16, 2017.

\*Address correspondence to: Costin N. Antonescu ([cantonescu@ryerson.ca](mailto:cantonescu@ryerson.ca)).

Abbreviations used:  $\beta$ 1-AR,  $\beta$ 1-adrenergic receptor; AP2, adaptor protein 2; BAPTA-AM, 1,2-bis(2-aminophenoxy)ethane-*N,N,N',N'*-tetraacetic acid tetrakis(acetoxymethyl ester); BIM, bisindolylmaleimide I; CCP, clathrin-coated pit; CLS, clathrin-labeled structure; CsA, cyclosporin A; DMSO, dimethyl sulfoxide; DR, death receptor; EGF, epidermal growth factor; eGFP, enhanced green fluorescent protein; EGFR, EGF receptor; ELISA, enzyme-linked immunosorbent assay; FBS, fetal bovine serum; GPCR, G-protein-coupled receptor; HA, hemagglutinin; IP3, inositol trisphosphate; MAPK, mitogen-activated protein kinase; MEF, mouse embryonic fibroblast; NFAT, nuclear factor of activated T-cells; PFA, paraformaldehyde; PH, pleckstrin homology; PI3K, phosphatidylinositol-3-kinase; PIP2, phosphatidylinositol-4,5-bisphosphate; PKC, protein kinase C; PLC, phospholipase C; PLC $\gamma$ 1, phospholipase C $\gamma$ 1; PMA, phorbol 12-myristate 13-acetate; RPE, retinal pigment epithelial (cells); sCLS, subthreshold clathrin-labeled structure; siRNA, small interfering RNA; Sjn1, synaptojanin1; Tfn, transferrin; TfR, transferrin receptor; TIRF-M, total internal reflection fluorescence microscopy; TRAIL, tumor necrosis factor-related apoptosis-inducing ligand; XcC, xestospingon C.

© 2017 Delos Santos et al. This article is distributed by The American Society for Cell Biology under license from the author(s). Two months after publication it is available to the public under an Attribution-Noncommercial-Share Alike 3.0 Unported Creative Commons License (<http://creativecommons.org/licenses/by-nc-sa/3.0>).

"ASCB"®, "The American Society for Cell Biology"®, and "Molecular Biology of the Cell"® are registered trademarks of The American Society for Cell Biology.

## INTRODUCTION

Clathrin-mediated endocytosis is the principal mechanism of internalization of receptor-bound macromolecules and integral membrane proteins (termed cargo) from the cell surface. As a result, clathrin is a key regulator of the cell-surface proteome and controls the interaction of eukaryotic cells with their environment. Clathrin, AP2, and many other proteins assemble into clathrin-coated pits (CCPs), small invaginating regions of the plasma membrane. CCPs lead to the formation of intracellular vesicles following scission from the plasma membrane by the GTPase dynamin2. For some receptors, clathrin-mediated endocytosis is a necessary part of nutrient uptake (e.g., of iron by transferrin receptor [TfR]) (Antonescu et al., 2014). For signaling receptors such as the epidermal growth factor receptor (EGFR), internalization can lead to eventual signal termination by lysosomal degradation (Goh and Sorkin, 2013).

The formation of CCPs spans several stages, including nucleation of clathrin-labeled structures (CLSs), followed by CCP initiation, assembly, maturation, and eventual scission (McMahon and Boucrot, 2011; Aguet et al., 2013; Mettlen and Danuser, 2014;

Kadlecova et al., 2017). In addition to clathrin, adaptor protein 2 (AP2), and dynamin, CCP formation is regulated by many other endocytic accessory proteins that are recruited to CCPs through interaction with clathrin, AP2, or other proteins (Schmid and McMahon, 2007; Mettlen et al., 2009; McMahon and Boucrot, 2011; Taylor et al., 2011). These include proteins that can sense or generate membrane curvature and enzymes such as synaptojanin1 (Sjn1), which controls the turnover of phosphatidylinositol-4,5-bisphosphate (PIP2). Indeed, PIP2 acts as a membrane ligand for many endocytic proteins, and ablation of PIP2 impairs formation of CCPs and clathrin-mediated endocytosis (Jost et al., 1998; Varnai et al., 2006; Zoncu et al., 2007). Specifically, PIP2 synthesis by phosphatidylinositol-5-kinases and turnover by lipid phosphatases such as Sjn1 regulates CCP initiation, assembly, size, and lifetime (Antonescu et al., 2011). Collectively CCPs are regulated by PIP2 and require the coordinated assembly of many proteins within CCPs to mediate efficient formation of clathrin-coated vesicles and thus internalization of receptor cargo.

Further to the well-described role of clathrin in endocytosis, recent studies have also uncovered a direct role for clathrin and CCPs in regulating and organizing receptor signaling at the plasma membrane. Activation of phosphatidylinositol-3-kinase (PI3K)-Akt signaling upon ligand binding by the EGFR requires clathrin but not receptor endocytosis (Garay et al., 2015; Lucarelli et al., 2016), indicating the requirement for enrichment of EGFR signals within CCPs at the cell surface. Further,  $\beta$ 1-adrenergic receptor ( $\beta$ 1-AR) agonist stimulation elicits enrichment of  $\beta$ -arrestin2 but not  $\beta$ 1-AR within cell-surface clathrin structures (Eichel et al., 2016), supporting the notion that CCPs function as signaling hubs.

Given the diversity of roles of clathrin at the cell surface, a fundamental question emerges: How can clathrin function be uniquely and specifically tailored to appropriately regulate the many distinct receptors at the cell surface? CCPs are heterogeneous in size, lifetime, and protein composition (Puthenveedu and von Zastrow, 2006; Liu et al., 2009, 2010; Loerke et al., 2009, 2011; Mettlen et al., 2009, 2010; Antonescu et al., 2010, 2011; Nunez et al., 2011; Taylor et al., 2011; Aguet et al., 2013). Several lines of evidence indicate that CCP heterogeneity reflects in part distinct cargo protein content. First, CCPs harboring specific proteins exhibit distinct size (e.g., larger CCPs form upon recruitment of low-density lipoprotein receptor (LDLR) and dab2/ARH; Mettlen et al., 2010) or longer lifetimes (e.g., upon recruitment of certain G-protein-coupled receptors [GPCRs]; Puthenveedu and von Zastrow, 2006). Second, the clathrin-mediated endocytosis of different cargo receptors has distinct functional requirements: EGFR but not TfR endocytosis is regulated by phosphatidic acid (Antonescu et al., 2010), while gene silencing or sequestration of AP2 strongly impairs TfR endocytosis but not that of EGFR in some cells (Conner and Schmid, 2003; Motley et al., 2003; Johannessen et al., 2006). In addition to having mechanistically distinct requirements for AP2 during clathrin-mediated endocytosis (Johannessen et al., 2006), it has been proposed that EGFR and TfR may be localized largely to distinct CCPs (Tosoni et al., 2005; Johannessen et al., 2006).

That CCPs can be functionally specialized for internalization of different receptors raises the important possibility that subsets of CCPs can be uniquely regulated, in turn regulating specific subset(s) of cargo receptors. Identifying signals that selectively regulate CCPs harboring specific cargoes would provide important understanding of how clathrin can distinctly regulate the diverse proteins at the cell surface.

Phospholipase C $\gamma$ 1 (PLC $\gamma$ 1) is one of the many signals activated by EGFR and other receptor tyrosine kinases. Activation of PLC $\gamma$ 1 is

complex and can occur via binding to tyrosine-phosphorylated EGFR at pY992 (Rotin et al., 1992) or indirectly, for example, via binding to the phosphorylated EGFR adaptor Gab1 (Gual et al., 2000). Once bound to a receptor complex, PLC $\gamma$ 1 is phosphorylated (Kadamur and Ross, 2013), thus increasing phosphodiesterase activity specific for PIP2, resulting in production of inositol trisphosphate (IP3) and diacylglycerol (Kadamur and Ross, 2013). By binding to the IP3 receptor on the endoplasmic reticulum, IP3 leads to an increase in cytosolic Ca<sup>2+</sup>.

In presynaptic neurons, exocytosis triggers rapid and robust exocytosis of synaptic vesicles, which is coupled to enhanced clathrin-mediated endocytosis. Several mechanisms contribute to the latter, including an increase in intracellular Ca<sup>2+</sup>, triggering the activation of the phosphatase calcineurin (Cousin, 2000; Cousin and Robinson, 2001; Saheki and De Camilli, 2012). In turn, calcineurin dephosphorylates a number of proteins, including dynamin1, Sjn1, amphiphysin 1 and 2, AP180, Epsin, and Eps15, which increases the pool of available endocytic proteins to enhance clathrin-mediated endocytosis (Liu et al., 1994; Bauerfeind et al., 1997; Slepnev et al., 1998; Chen et al., 1999; Cousin and Robinson, 2001; Cousin et al., 2001; Saheki and De Camilli, 2012). However, neurons express many unique isoforms or elevated levels of certain endocytic proteins and thus have specialized clathrin-mediated endocytosis (Morris and Schmid, 1995; Saheki and De Camilli, 2012).

The role of Ca<sup>2+</sup> in controlling clathrin in nonneuronal cells remains poorly understood. Earlier studies showed that EGFR endocytosis is largely unimpaired in PLC $\gamma$ 1<sup>-/-</sup> mouse embryonic fibroblasts (MEFs) (Ji et al., 1998) and that EGF-dependent Ca<sup>2+</sup> mobilization is not required for EGFR internalization (Chang et al., 1991). In contrast, other studies suggested Ca<sup>2+</sup> signals may regulate EGFR endocytosis (Korc et al., 1984). EGFR is capable of endocytosis by both clathrin-dependent and nonclathrin mechanisms (Sigismund et al., 2008). Thus study of how PLC $\gamma$ 1-Ca<sup>2+</sup> signals may control the clathrin-mediated endocytosis of EGFR requires examination of this phenomenon in cells in which EGFR endocytosis is very largely clathrin-dependent and the use of highly sensitive assays that can monitor the impact of PLC $\gamma$ 1-Ca<sup>2+</sup> signals on EGFR endocytosis and CCP dynamics.

By activating PLC $\gamma$ 1, EGFR may thus regulate clathrin-dependent signaling and endocytosis by consuming PIP2 or by generating secondary IP3-dependent Ca<sup>2+</sup> signaling. Here we examine how signals triggered by PLC $\gamma$ 1 regulate clathrin-mediated endocytosis by monitoring receptor internalization and by employing highly sensitive microscopy assays to resolve the impact of PLC $\gamma$ 1-Ca<sup>2+</sup> signals on receptor endocytosis and CCP dynamics. We use these approaches to probe how PLC $\gamma$ 1 signals may selectively control discrete subsets of CCPs (e.g., harboring EGFR) but not others (e.g., involved in constitutive endocytosis of TfR).

## RESULTS

### PLC $\gamma$ 1 selectively controls clathrin-mediated endocytosis of EGFR

EGF stimulation of retinal pigment epithelial (ARPE-19, henceforth RPE) cells elicits phosphorylation and thus activation of PLC $\gamma$ 1, detectable as early as 1 min after ligand addition (Supplemental Figure 1A). To determine whether PLC $\gamma$ 1 signaling contributes to EGFR or TfR clathrin-mediated endocytosis, we used small interfering RNA (siRNA)-mediated silencing of PLC $\gamma$ 1 in RPE cells, which resulted in an 85.6  $\pm$  6.4% reduction ( $p < 0.05$ ,  $n = 3$ ) in PLC $\gamma$ 1 expression (Supplemental Figure 1B), and monitored internalization of the respective receptor ligands EGF and transferrin (Tfn). PLC $\gamma$ 1 silencing impaired the internalization of EGF (Figure 1A) but had no effect on

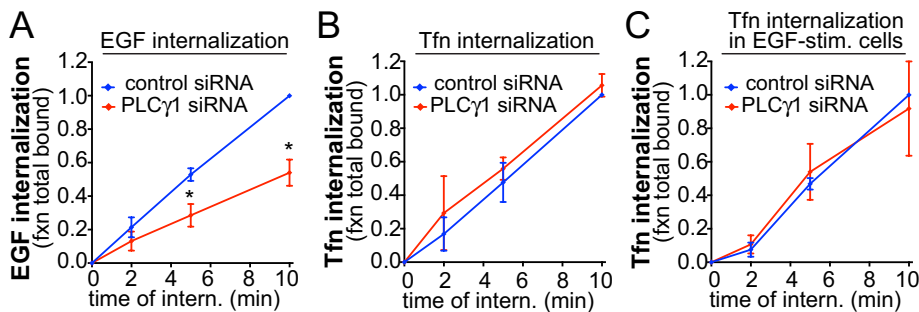


**FIGURE 1:** PLC $\gamma$ 1 is required for EGF but not Tfn internalization. RPE cells were treated with siRNA targeting PLC $\gamma$ 1 or nontargeting siRNA, followed by measurement of EGF (A), Tfn (B), or Tfn internalization in EGF-stimulated cells (C). Shown are the means  $\pm$  SE for  $n > 3$  independent experiments; \*,  $p < 0.05$ .

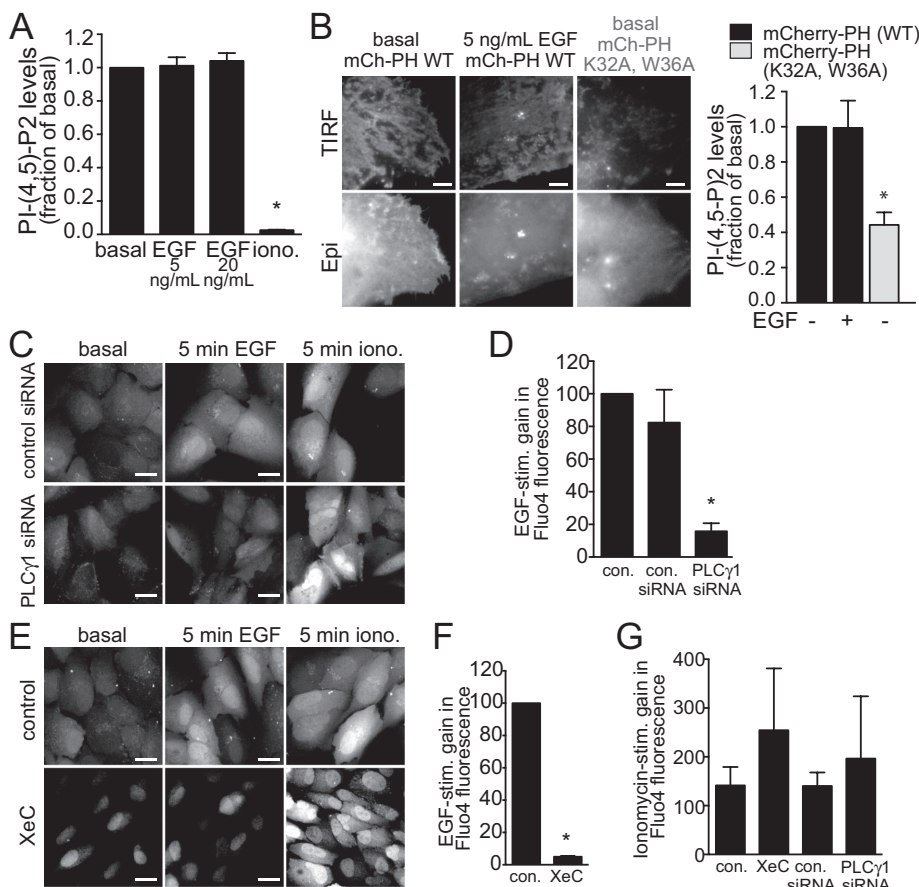


**FIGURE 2:** EGF stimulation elicits a PLC $\gamma$ 1-dependent increase in cytosolic Ca<sup>2+</sup>. (A) Biochemical PIP2 measurement (means  $\pm$  SE) in cells treated with EGF (5 or 20 ng/ml, 5 min) or ionomycin (10  $\mu$ M, 20 min) as indicated.  $n = 3$ ; \*,  $p < 0.05$ . (B) RPE cells transfected with cDNA encoding the wild-type PH domain of PLC $\delta$ 1 fused to mCherry (mCh-PH WT) or a similar fusion with a K32A/W36A mutant PH domain (unable to bind PIP2; Antonescu et al., 2011). Shown are representative micrographs obtained by wide-field epifluorescence or TIRF microscopy, as indicated and the means  $\pm$  SE of the TIRF/epifluorescence ratio of the mCherry signal, indicative of membrane binding by the PH probe. (C–G) RPE cells were treated with siRNA targeting PLC $\gamma$ 1 or nontargeting siRNA, or treated with 3  $\mu$ M XeC for 20 min or left untreated (control). RPE cells were then treated with Fluo4-AM for 30 min. Shown in C and E are representative images obtained by wide-field epifluorescence of Fluo4 obtained before further treatments (basal), after stimulation with 5 ng/ml EGF for 5 min, and then again after subsequent treatment with 10  $\mu$ M ionomycin for 5 min, as indicated. Scale bars: 20  $\mu$ m. Also shown are the EGF-stimulated (D, F) or ionomycin triggered (G) gains (means  $\pm$  SE) in Fluo4-AM fluorescence within cells in the various conditions examined.  $n > 3$ , \*,  $p < 0.05$ .

that of Tfn (Figure 1B). Strikingly, the lack of effect of PLC $\gamma$ 1 silencing on the endocytosis of Tfn was observed even in the presence of EGF stimulation (Figure 1C), ruling out a broad effect of PLC $\gamma$ 1 on clathrin-mediated endocytosis (e.g., of Tfr) only in EGF-stimulated cells.

In some cells, EGFR may undergo clathrin-independent endocytosis upon stimulation with high levels of EGF (>20 ng/ml) (Sigismund et al., 2008). Importantly, for all experiments, we monitored EGFR internalization at low doses of EGF stimulation (5 ng/ml) to favor receptor internalization by clathrin-mediated endocytosis (Sigismund et al., 2008). Indeed, we have previously characterized that in RPE cells, this results in EGFR internalization occurring very largely by clathrin-mediated endocytosis (Garay et al., 2015). Moreover, even at saturating levels of EGF stimulation (100 ng/ml EGF), the internalization of EGFR is predominantly clathrin dependent in RPE cells (Supplemental Figure 2A). This indicates that, in RPE cells, EGFR may be largely restricted to internalization by clathrin-mediated endocytosis. We conclude that PLC $\gamma$ 1 selectively controls the clathrin-dependent endocytosis of EGFR.

### PLC $\gamma$ 1-derived intracellular calcium is selectively required for clathrin-mediated endocytosis of EGFR

PLC $\gamma$ 1 may control EGFR endocytosis by consumption of PIP2 or by generation of secondary signaling intermediates such as intracellular Ca<sup>2+</sup>. PLC $\gamma$ 1 has also been proposed to regulate endocytosis by acting as a guanyl exchange factor for dynamin1 in neuronal cells (Choi et al., 2004), and dynamin1 selectively regulates the clathrin-mediated endocytosis of tumor necrosis factor-related apoptosis-inducing ligand (TRAIL)-death receptor (DR) (Reis et al., 2017). However, silencing of dynamin1 in RPE cells had no effect on EGF internalization (Supplemental Figure 3, A and B), indicating that PLC $\gamma$ 1-regulated EGFR clathrin-mediated endocytosis is dynamin1-independent. Notably, EGFR internalization in RPE cells requires dynamin2 (Garay et al., 2015), which has not been reported to be directly controlled by PLC $\gamma$ 1.

Further, under these conditions, EGF stimulation did not appreciably decrease PIP2 levels, as detected by biochemical measurement of PIP2 levels at low (5 ng/ml) or higher (20 ng/ml) EGF doses (Figure 2A). Consistent with this result, monitoring PIP2 availability using a genetically encoded fluorescent PIP2 probe coupled to total internal reflection fluorescence microscopy (TIRF-M) indicated that EGF stimulation did not appreciably decrease the fluorescence levels

of this probe in the TIRF field (Figure 2B), a reflection of the PIP2-dependent membrane association of the probe. As this probe is largely associated with the plasma membrane in resting (basal) cells, this method likely does not allow detection of possible increases in PIP2 compared with control cells. Nonetheless, these experiments indicate that the impact of PLC $\gamma$ 1 on EGFR endocytosis is not due to robust, broad PIP2 depletion.

In contrast, and as expected (Fu *et al.*, 1994; Bryant *et al.*, 2004), EGF stimulation increased cytosolic [Ca $^{2+}$ ], as detected by a gain in fluorescence of the Ca $^{2+}$  probe Fluo4-AM (Figure 2C). Importantly, the EGF-stimulated gain in Fluo4-AM fluorescence was ablated by PLC $\gamma$ 1 silencing (Figure 2, C and D) or by treatment with the IP3 receptor inhibitor Xestospongine C (XeC) (Oka *et al.*, 2002) (Figure 2, E and F). In each of these PLC $\gamma$ 1- or IP3 receptor-perturbing conditions, subsequent treatment with the calcium ionophore ionomycin elicited a robust increase in intracellular Ca $^{2+}$  (Figure 2G), indicating that these treatments did not alter Fluo4-AM uptake. Hence PLC $\gamma$ 1 and the IP3 receptor are required for the EGF-stimulated gain in cytosolic Ca $^{2+}$ .

The selective requirement for PLC $\gamma$ 1 in EGFR internalization may thus reflect a selective requirement for IP3-derived Ca $^{2+}$  signaling elicited by EGF stimulation. Indeed, treatment with XeC abrogated EGF internalization (Figure 3A), again without affecting Tfn internalization either in the absence (Figure 3B) or presence (Figure 3C) of EGF stimulation. Identical results were obtained using BAPTA-AM (1,2-bis(2-aminophenoxy)ethane-*N,N,N',N'*-tetraacetic acid tetrakis(acetoxymethyl ester)) to chelate intracellular calcium (Figure 3, D–F). BAPTA-AM treatment did not impact the total amount of cell-associated EGF when the assay was repeated without distinguishing internalized from surface-associated EGF (Supplemental Figure 2B). This indicates that BAPTA-AM treatment did not impact EGF internalization as a result of alteration of EGF:EGFR association but instead decreased the rate of EGF:EGFR internalization. Hence IP3-stimulated Ca $^{2+}$  release from the endoplasmic reticulum is selectively required for the clathrin-dependent internalization of EGFR.

To examine how PLC $\gamma$ 1-derived Ca $^{2+}$  signals may selectively control EGFR clathrin-mediated endocytosis, we first examined

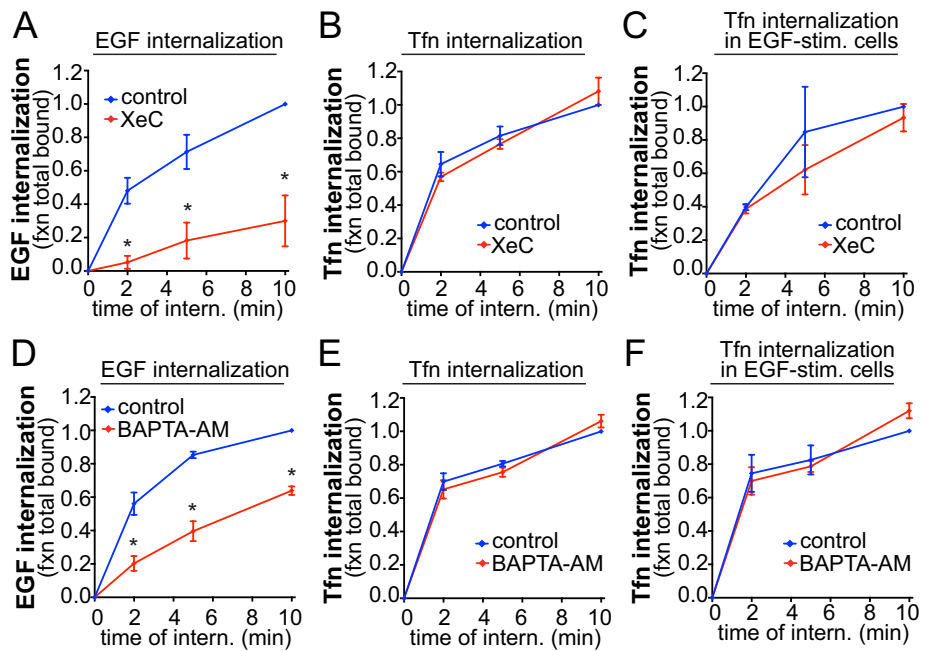


**FIGURE 3:** IP3 receptor and cytosolic Ca $^{2+}$  are required for EGF but not Tfn internalization. RPE cells were treated with 3  $\mu$ M XeC for 30 min, 10  $\mu$ M BAPTA-AM for 15 min, or left untreated (control) as indicated, followed by measurement of EGF (A, D), Tfn (B, E) or Tfn internalization in EGF-stimulated cells (C, F). Shown are the means  $\pm$  SE for  $n > 3$  independent experiments; \*,  $p < 0.05$ .

whether this recapitulated the neuronal control of endocytosis by calcium-activated calcineurin. Strikingly, the calcineurin inhibitor cyclosporin A (CsA) was without effect on EGF internalization (Figure 4A), while under similar conditions, CsA effectively impaired the calcineurin-dependent nuclear translocation of nuclear factor of activated T-cells (NFAT; Supplemental Figure 3, C and D). These results indicate that the mechanism of regulation of EGFR endocytosis in RPE cells is at least partly distinct from that of enhanced clathrin-mediated endocytosis elicited by Ca $^{2+}$  signaling in neurons.

Ca $^{2+}$  signaling activates several signals, including conventional protein kinase C (PKC) isoforms. To determine whether Ca $^{2+}$ -dependent PKC activation contributes to EGFR endocytosis, we employed the pan-PKC inhibitor bisindolylmaleimide I (BIM). EGF internalization was impaired in cells treated with BIM (Figure 4B), while BIM treatment was without effect on Tfn internalization, measured either in the absence (Figure 4C) or presence (Figure 4D) of EGF stimulation. Hence PKC selectively

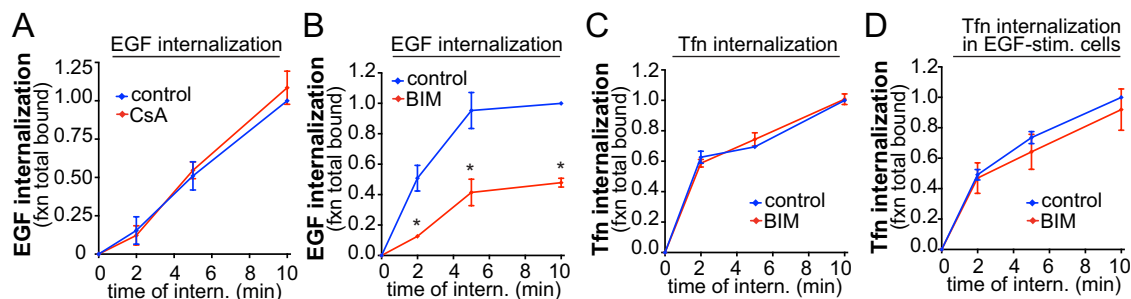


**FIGURE 4:** PKC, but not calcineurin, is selectively required for EGF internalization. RPE cells were treated with 10  $\mu$ M CsA for 30 min or 1  $\mu$ M BIM for 30 min, or left untreated (control), followed by measurement of EGF (A, B), Tfn (C), or Tfn internalization in EGF-stimulated cells (D). Shown are the means  $\pm$  SE for  $n > 3$  independent experiments; \*,  $p < 0.05$ .

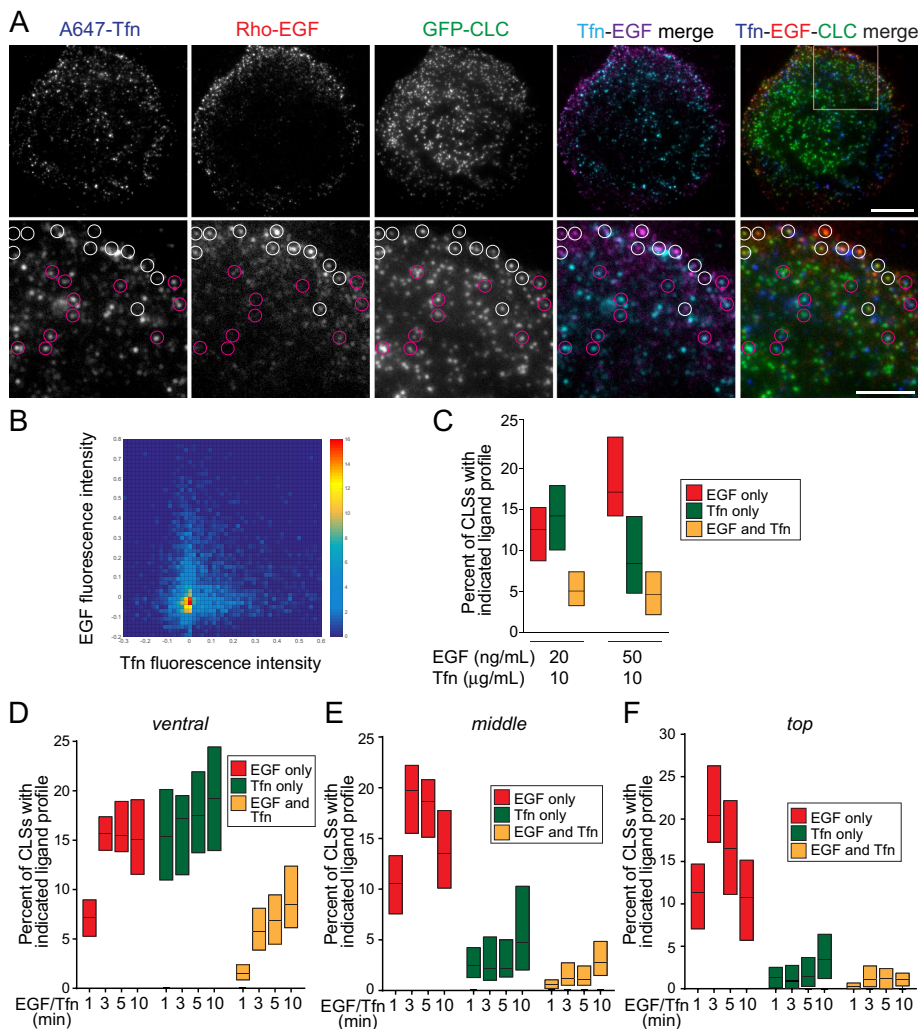


**FIGURE 5:** EGF and TfR are recruited to largely distinct CLSs. RPE cells stably expressing clathrin light chain fused to eGFP (eGFP-CLCa) were treated with 20 ng/ml rhodamine-EGF (rho-EGF) and 10  $\mu$ g/ml A647-Tfn for 5 min or the indicated time, followed by immediate fixation. (A) Shown are representative micrographs obtained by TIRF-M. Scale bars: 10  $\mu$ m (top row); 5  $\mu$ m (bottom row), corresponding to enlarged images of the region shown in the merged image of the top row. White circles depict CLSs that are positive for EGF but devoid of TfR, and purple circles depict CLSs that are positive for TfR but not EGF. (B, C) CLSs were subjected to automated detection and analysis as described in *Materials and Methods*. Shown in B is a two-dimensional histogram of the normalized EGF and TfR fluorescence intensities in each CLS cohort. Shown in C are median (bar) and 25th/75th percentiles (boxes) of the proportions of CLSs that are positive for EGF (but not TfR), TfR (but not EGF), or both EGF and TfR. The number of CLSs and cells analyzed, for each condition are as follows: 10 ng/ml rhodamine-EGF and 10  $\mu$ g/ml A647-Tfn: 70,124 and 57; and 10 ng/ml rhodamine-EGF and 10  $\mu$ g/ml A647-Tfn: 46,240 and 37; from a minimum of three independent experiments in each condition. (D–F) Images obtained by spinning-disk confocal microscopy, corresponding to ventral (D), middle (E), and top (F) z-sections of cells (see Supplemental Figure 5 for representative images) were subjected to automated detection and analysis as described in *Materials and Methods*. Shown are median (bar) and 25th/75th percentiles (boxes) of the proportions of CLSs in the ventral (D), middle (E), and top (F) z-sections that are positive for EGF (but not TfR), TfR (but not EGF), or both EGF and TfR. The number of CLSs analyzed and cells for each condition (from three independent experiments) are provided in the legend for Supplemental Figure 5.

regulates the clathrin-dependent internalization of EGFR in a manner similar to PLC $\gamma$ 1- and ER-derived cytosolic Ca<sup>2+</sup>.

### EGFR and TfR localize largely to distinct CLSs

Our results indicate that the clathrin-mediated endocytosis of EGFR and TfR has distinct requirements for PLC $\gamma$ 1-derived Ca<sup>2+</sup> signals,

including PKC. This is consistent with the distinct requirements for clathrin-dependent EGFR and TfR internalization for AP2 (Conner and Schmid, 2003; Motley et al., 2003), phosphatidic acid (Antonescu et al., 2010), or TTP (Tosoni et al., 2005). These results lead to the hypothesis that EGFR and TfR reside within distinct subpopulations of clathrin structures (Tosoni et al., 2005; Leonard et al., 2008), each with distinct functional requirements. To directly and systematically probe this possibility, we performed simultaneous labeling of RPE cells stably expressing clathrin light chain fused to enhanced green fluorescent protein (eGFP) (eGFP-CLCa) with the fluorescently conjugated ligands of TfR and EGFR, rhodamine-EGF and A647-Tfn (ligands added for 5 min, followed by fixation), respectively (Figure 5). This labeling approach was coupled to TIRF-M, allowing observation of diffraction-limited clathrin structures and their respective receptor content (Figure 5A). Here we use the term clathrin-labeled structures (CLSs) for clathrin structures observed or detected within single images (frames); identification of bona fide CCPs requires additional analysis of CLS behavior over time that is possible only when examining live-cell images (Aguet et al., 2013; Kadlecova et al., 2017). The set of CLSs includes CCPs as well as other clathrin structures such as subthreshold CLSs (sCLSs), of which the latter do not give rise to bona fide CCPs (Aguet et al., 2013; Mettlen and Danuser, 2014; Kadlecova et al., 2017). In these images (Figure 5A), CLSs harboring either EGFR (white circles) or TfR (purple circles) can be readily observed, while CLSs harboring both receptors are more rare.

To obtain quantitative analysis of the relationship between EGFR-positive and TfR-positive CLSs, we subjected these TIRF-M images to automated detection and analysis of CLSs (Jaqaman et al., 2008; Loerke et al., 2009; Mettlen et al., 2009, 2010, Antonescu et al., 2010, 2011; Liu et al., 2010; Aguet et al., 2013; Garay et al., 2015). Importantly, this strategy allows unbiased and systematic identification of CLSs, as well as measurement of the levels of fluorescent receptors contained therein (Aguet et al., 2013; Garay et al., 2015; Lucarelli et al., 2016). To represent these data, we first plotted the distribution of fluorescent EGF and TfR within all identified CLSs in a two-dimensional histogram (Figure 5B). Importantly, this approach reveals an apparently mutually exclusive relationship between the content of EGF and TfR within CLSs. To directly quantify the proportion of CLSs that contain EGFR (EGF+), TfR (TfR+), or both receptors (EGF+/TfR+), we sorted CLSs into cohorts by receptor content, using a systematic cutoff for classification of CLSs as positive for EGFR

or Tfn (Garay *et al.*, 2015). Importantly, this approach revealed that CLSs harboring either EGF or Tfn (but not both ligands) were approximately threefold more abundant than CLSs harboring both receptors (Figure 5C). Using higher concentrations of rhodamine-EGF (50 ng/ml) increased the percentage of EGF+ CLSs, without altering the percentage of EGF+/Tfn+ CLSs (Figure 5C). Quantification of the ligand content of each cohort of CLSs (EGF+, Tfn+, EGF+/Tfn+) highlights the validity of the automated sorting of CLSs by cargo content (Supplemental Figure 4). These results indicate that EGFR and Tfr are found largely in distinct CLSs and thus may internalize largely through distinct CCPs.

While we observed both EGFR+ and Tfr+ CLSs on the ventral cell surface (as imaged by TIRF-M), others have reported that Tfr internalization occurs largely on the ventral cell surface and that of EGFR occurs largely on the dorsal cell surface (Grossier *et al.*, 2014). As such, it is possible that CLSs harboring both EGFR and Tfr may predominate on the dorsal cell surface, given the possible enrichment of EGFR internalization events in this region. Furthermore, while Tfr undergoes constitutive endocytosis, EGFR internalization is triggered by ligand binding, suggesting that the recruitment of EGFR and Tfr to distinct or overlapping CLSs may depend on the time of addition of ligands. To probe these possibilities, we repeated these experiments using a similar labeling strategy to detect EGFR and Tfn, followed by imaging by spinning-disk confocal microscopy. This approach allows a similar systematic, unbiased analysis of ligand recruitment to CLSs (detected via AP2 staining) in various z-sections of cells, including the ventral section (which is analogous to the analysis performed by TIRF-M) and two dorsal sections (corresponding to the middle and top of the cell). As virtually all cell-surface CCPs have AP2 (Keyel *et al.*, 2006), we also refer to these AP2 structures as CLSs (Supplemental Figure 10). As observed by TIRF-M, CLSs harboring either EGFR (white circles) or Tfr (purple circles) can be readily observed in these sections, while CLSs harboring both receptors are less frequently observed (Supplemental Figure 5).

Following automated detection, analysis, and sorting of CLSs into cohorts by ligand (EGF+, Tfn+ and EGF+/Tfn+), we again observed that CLSs harboring either EGF or Tfn (but not both ligands) were approximately threefold more abundant than CLSs harboring both receptors in the images corresponding to the ventral section of cells (Figure 5D). Consistent with previous reports showing the abundance of EGFR on the dorsal surface of cells, we observed a substantial number of EGF+ CCPs on the middle and top sections of cells, while Tfn+ CCPs were less abundant, and CLSs harboring both EGF and Tfn were virtually absent in these dorsal cell sections (Figure 5, E and F). Notably, while the frequency of detection of EGF+ CLSs (and EGF+/Tfn+ CLSs) was lower at 1 min of ligand addition, the approximately threefold higher abundance of EGF+ versus EGF+/Tfn+ CLSs is similar at all time points following ligand addition examined. Quantification of the ligand content of each cohort of CLSs (EGF+, Tfn+, EGF+/Tfn+) highlights the validity of the automated sorting of CLSs by cargo content (Supplemental Figure 6).

Collectively these systematic analyses of the recruitment of Tfn and EGF ligands to CLSs indicates that Tfr and EGFR reside largely in distinct CLSs. This phenomenon is not dependent on the time of EGF or Tfn addition and occurs throughout the plasma membrane (*i.e.*, in both the ventral and the dorsal surfaces of cells). These results suggest that EGFR and Tfr internalize largely through distinct CCPs.

### EGFR-derived Ca<sup>2+</sup> signals regulate CCP initiation and assembly

We next examined how CCPs harboring EGFR or Tfr may be distinctly regulated by PLC $\gamma$ 1-derived Ca<sup>2+</sup> signals. The requirement

for Ca<sup>2+</sup>-signaling for EGFR clathrin-mediated endocytosis may reflect a role for Ca<sup>2+</sup> in EGFR recruitment to CLSs or a role for Ca<sup>2+</sup> signaling in CCP nucleation, initiation, assembly, maturation, or scission subsequent to receptor recruitment therein (Antonescu *et al.*, 2010, 2011; Aguet *et al.*, 2013; Mettlen and Danuser, 2014; Garay *et al.*, 2015; Kadlecova *et al.*, 2017).

To determine whether Ca<sup>2+</sup> signaling was required for EGFR recruitment to CLSs, we treated cells with a pulse (5 min) of fluorescent EGF coupled to imaging by TIRF-M and automated detection and analysis of CLSs (Aguet *et al.*, 2013; Garay *et al.*, 2015). We performed parallel experiments with fluorescent EGF (A555-EGF, Figure 6, A, C, and D, and Supplemental Figure 7) and Tfn (A555-Tfn, Figure 6, B, E, and F, and Supplemental Figure 7). Cells treated with XeC, BAPTA-AM, or BIM exhibited an increase in EGF fluorescence within CLSs (Figure 6C), indicating that EGFR was efficiently recruited to and accumulates in CLSs under these conditions. Thus Ca<sup>2+</sup>-PKC signaling was required for a stage of clathrin-mediated endocytosis subsequent to EGFR recruitment to CLSs. Importantly, and consistent with ligand-uptake experiments (Figures 3 and 4), XeC, BAPTA-AM, and BIM treatments did not impact Tfn recruitment to CLSs (Figure 6E), showing that the effect of Ca<sup>2+</sup>-PKC signaling is selective for EGFR localization to CLSs. Notably, the fluorescence intensity of clathrin within EGF+ CLSs (Figure 6D) but not that of Tfn+ CLSs (Figure 6F) was reduced upon treatment with either XeC, BAPTA-AM, or BIM, suggesting that Ca<sup>2+</sup>-PKC signaling regulates a process of CCP formation or assembly other than EGFR recruitment.

To resolve how Ca<sup>2+</sup> signals may regulate the nucleation, initiation, assembly, maturation, or scission of CCPs harboring EGFR, we used established approaches that couple time-lapse TIRF-M imaging of cells and automated and unbiased detection, tracking, and analysis of CLSs (Aguet *et al.*, 2013; Mettlen and Danuser, 2014; Kadlecova *et al.*, 2017). Using these approaches, we examined RPE cells stably expressing GFP-CLC, treated (or not) with BAPTA-AM and imaged in the presence of either rhodamine-EGF or A647-Tfn (the latter in the presence of unlabeled EGF to trigger Ca<sup>2+</sup> signaling) (Figure 7, A and B). Notably, these computational tools allow the identification of clathrin structures harboring specific receptors in two-color time lapse-image series, based on the presence of a secondary signal within these structures (Aguet *et al.*, 2013). As such, this method allows the selective analysis of EGF+ or Tfn+ CLSs in these time lapse-image series. Furthermore, this method allows further resolution of each CLS as either a bona fide CCP or an sCLS, as previously described (Aguet *et al.*, 2013; Mettlen and Danuser, 2014; Kadlecova *et al.*, 2017). sCLSs are quantitatively and systematically distinguished from CCPs by the fact that sCLSs fail to meet a minimum clathrin-intensity threshold within the early stages of formation and likely represent either stochastic assembly of clathrin at the plasma membrane or early nucleation events that fail to proceed to formation of bona fide CCPs (Aguet *et al.*, 2013; Mettlen and Danuser, 2014; Kadlecova *et al.*, 2017). In contrast, bona fide CCPs represent CLSs that stabilize, assemble, mature, and, in some cases, undergo scission from the plasma membrane to produce vesicles.

Using this analysis strategy, we found that BAPTA-AM treatment significantly increased the rate of initiation of sCLSs containing EGF+ (Figure 7C) (Aguet *et al.*, 2013; Mettlen and Danuser, 2014; Kadlecova *et al.*, 2017). Importantly, BAPTA-AM substantially and significantly impaired the initiation of bona fide EGF+ CCPs (Figure 7D). This suggests that Ca<sup>2+</sup> signals control the transition from early nucleation to initiation of bona fide CCPs that contain EGFR. Furthermore, BAPTA-AM treatment decreased the size of bona fide CCPs containing EGF (EGF+ CCPs), shown by the

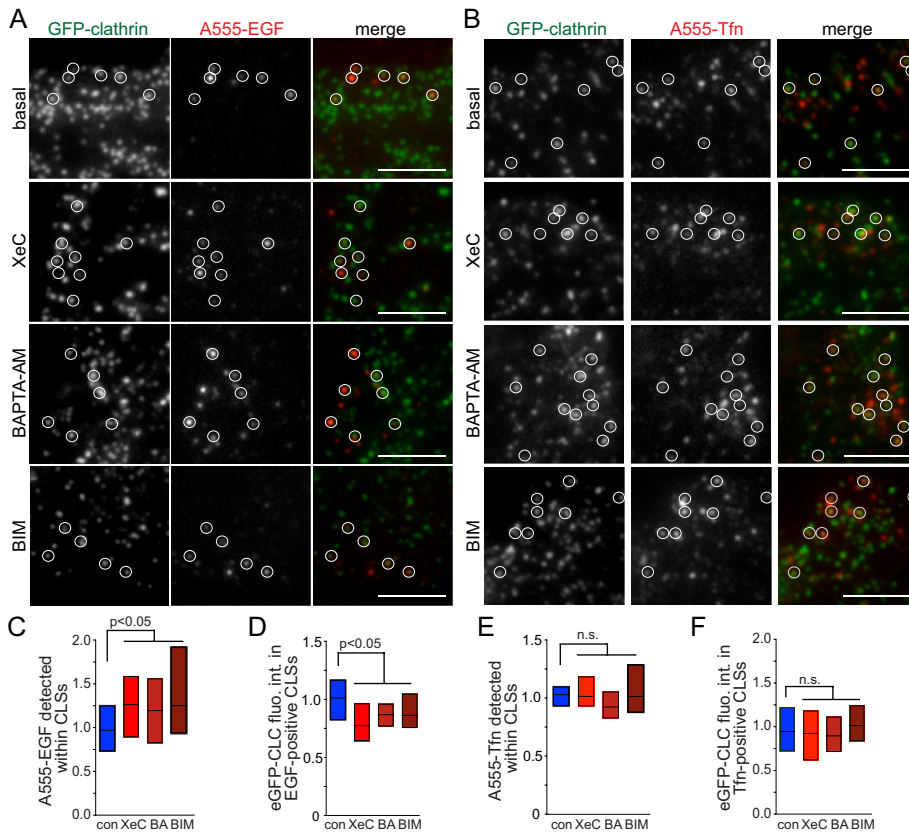


**FIGURE 6:** Cytosolic  $\text{Ca}^{2+}$  and PKC regulate CLSs containing EGFR but not those harboring TfR. RPE cells stably expressing clathrin light chain fused to eGFP (eGFP-CLCa), treated with various inhibitors as in Figures 3 and 4: 3  $\mu\text{M}$  XeC for 30 min, 10  $\mu\text{M}$  BAPTA-AM (BA) for 15 min, 1  $\mu\text{M}$  BIM for 30 min, or left untreated (control), and then treated with A555-EGF (A) or A555-Tfn (B) for 5 min. Shown are representative micrographs obtained by TIRF-M. Scale bar: 5  $\mu\text{m}$ . Full image panels are shown in Supplemental Figure 7. (C–F) TIRF-M images were subjected to automated detection of CLSs, followed by quantification of mean A555-conjugated ligand fluorescence intensity therein (C, E). CLSs were sorted into A555-EGF-enriched or A555-Tfn-enriched cohorts, followed by quantification of the mean eGFP-CLC within each CLS cohort (D, F). For C–F, the overall median of the cellular means (bar) and 25th/75th percentiles (boxes) are shown. The number of CLSs and cells analyzed, respectively, for each condition are as follows: EGF control: 14,114 and 114; EGF XeC: 11,322 and 98; EGF BAPTA-AM: 15,786 and 104; EGF BIM: 3860 and 46, Tfn control: 16,983 and 117; Tfn XeC: 10,838 and 98; Tfn BAPTA-AM: 8868 and 64; Tfn BIM: 3718 and 44; from a minimum of three independent experiments in each condition.

mean fluorescence of clathrin within CCPs, grouped by lifetime cohorts (Figure 7E). In contrast to the effects on EGF+ CLSs, BAPTA-AM treatment did not affect initiation rate of Tfn+ sCLSs or CCPs (Figure 7, F and G). BAPTA-AM also did not appreciably alter the size of Tfn+ CCPs (Figure 7H). As expected for CCPs giving rise to endocytic vesicles, the EGF or Tfn fluorescence decays from the detected objects largely concomitantly with clathrin (Supplemental Figures 8, A and B, and 9, A and B), in particular for CCPs having lifetimes <80s that represent the majority structures (Supplemental Figures 8C and 9C).

These results indicate that  $\text{Ca}^{2+}$  signals are selectively required to regulate the initiation and assembly of CCPs harboring EGFR following clathrin structure nucleation, while these  $\text{Ca}^{2+}$  signals are dispensable for the initiation and assembly of CCPs harboring TfR. Taken together with the observation that perturbation of  $\text{Ca}^{2+}$  signals enhances the abundance of EGFR within all CLSs (Figure 6C), these results indicate that  $\text{Ca}^{2+}$  signals do not impact recruitment of EGFR to clathrin structures, but are required for initiation and assembly of bona fide CCPs containing EGFR from nascent clathrin structures.

The initiation, assembly, maturation, and scission of CCPs require the recruitment and function of multiple endocytic accessory proteins that interact with clathrin heavy chain, AP2, or PIP2 (Schmid and McMahon, 2007; McMahon and Boucrot, 2011; Mettlen *et al.*, 2009; Taylor *et al.*, 2011). Manipulations that impact PIP2 synthesis and turnover by lipid kinases and CCP-localized phosphatases (Antonescu *et al.*, 2011) or that specifically alter the interactions of AP2 with PIP2 (Kadlecova *et al.*, 2017) impact CCP initiation and assembly. While systematic profiling of the recruitment of many such proteins is beyond the scope of this study, given the similarities of the impact of disruption of CCP-localized PIP2 dynamics or binding and disruption of  $\text{Ca}^{2+}$  signals, we next examined the regulation of the recruitment of Sjn1 by  $\text{Ca}^{2+}$  signals. Sjn1 effects localized PIP2 turnover within CCPs and thus negatively regulates the early stages of CCP formation (Antonescu *et al.*, 2011). We transfected cells with mCherry-tagged Sjn1 (mCh-Sjn1) and subjected these cells to imaging by TIRF-M (Figure 8A and Supplemental Figure 10) followed by systematic image analysis to quantify mCh-Sjn1 abundance within CLSs (Figure 8B). Strikingly, EGF stimulation resulted in a reduction of mCh-Sjn1 abundance within CLSs (Figure 8A and quantification in Figure 8B). Importantly, treatment with BAPTA-AM or BIM impaired the reduction of mCh-Sjn1 within CLSs elicited by EGF stimulation (Figure 8B). We obtained similar results by examination of endogenous Sjn1 labeled with anti-Sjn1 antibodies (Supplemental Figure 11). In addition, BAPTA-AM and BIM treatment also further increased Sjn1 labeling in CLSs beyond that in control, unstimulated cells in some conditions (Supplemental Figure 11), suggesting that the recruitment of endogenous Sjn1 may be further modulated by  $\text{Ca}^{2+}$  cues. These results are consistent with the observation that  $\text{Ca}^{2+}$ -derived signals are required for clathrin assembly within CCPs harboring EGFR and indicate that the  $\text{Ca}^{2+}$ -derived signals elicited by EGF stimulation more broadly remodel the assembly of CCPs, thus selectively regulating the clathrin-mediated endocytosis of specific cargo receptors such as EGFR.

These results are consistent with the observation that  $\text{Ca}^{2+}$ -derived signals are required for clathrin assembly within CCPs harboring EGFR and indicate that the  $\text{Ca}^{2+}$ -derived signals elicited by EGF stimulation more broadly remodel the assembly of CCPs, thus selectively regulating the clathrin-mediated endocytosis of specific cargo receptors such as EGFR.

### PLC $\gamma$ 1 is required for clathrin-dependent EGFR signaling

We recently reported that clathrin structures have a role separate from endocytosis in facilitating EGF-stimulated phosphorylation of Gab1 and Akt at the plasma membrane (Garay *et al.*, 2015). The role for clathrin structures in regulating signaling is selective, as clathrin is not required for EGF-stimulated phosphorylation of EGFR or Erk (Garay *et al.*, 2015). Given the role of PLC $\gamma$ 1-derived  $\text{Ca}^{2+}$  signals in controlling formation of EGFR-positive CCPs, we examined whether PLC $\gamma$ 1 controls EGFR signaling to Akt. PLC $\gamma$ 1 silencing impaired EGF-stimulated Gab1 and Akt phosphorylation (Figure 9A) but not that of EGFR and Erk (Figure 9B). Similarly, selective effects on EGFR

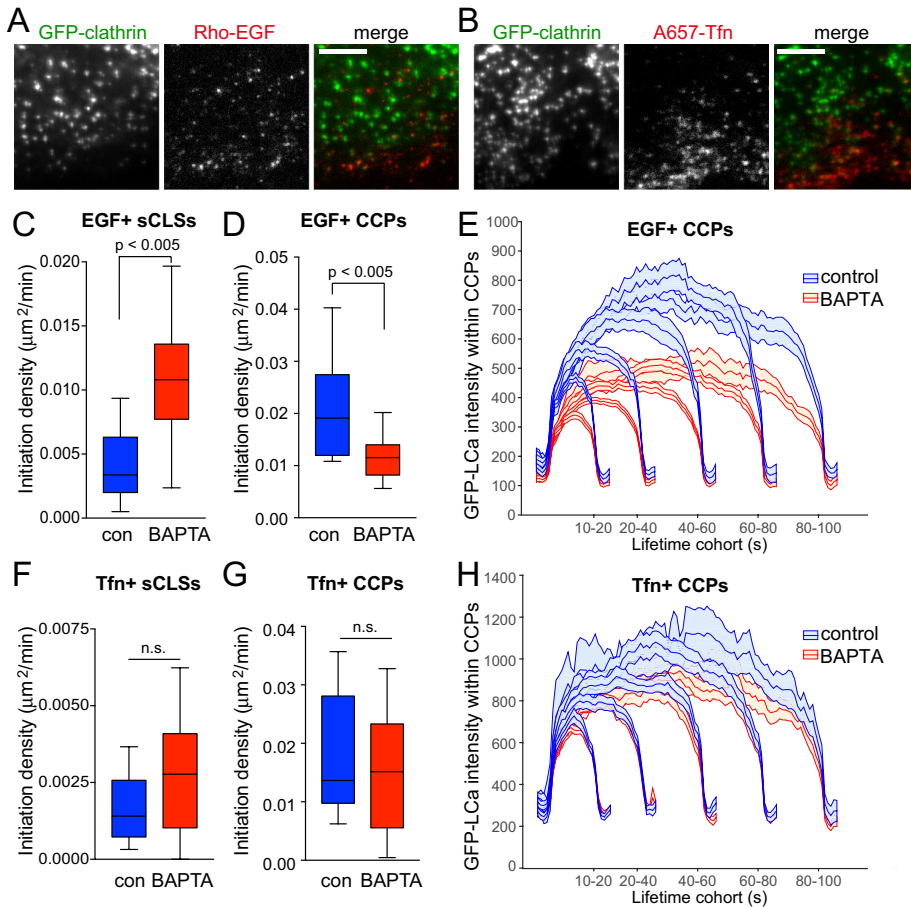


**FIGURE 7:** Cytosolic  $\text{Ca}^{2+}$  selectively controls initiation and assembly of CCPs harboring EGFR. RPE cells stably expressing clathrin light chain fused to eGFP (eGFP-CLCa) were pretreated with 10  $\mu\text{M}$  BAPTA-AM for 15 min, and then treated with either 20 ng/ml rhodamine-EGF (Rho-EGF) or treated with A647-Tfn during time-lapse imaging by TIRF-M. (A, B) Single-frame representative fluorescence micrographs. Scale bar: 5  $\mu\text{m}$ . Time-lapse TIRF-M image series of cells treated with Rho-EGF (C–E) or A647-Tfn (F–H) were subjected to automated detection, tracking, and analysis of CLSs as described in *Materials and Methods*, allowing identification of sCLSs and bona fide CCPs as EGF+ or Tfn+, as appropriate. (C–D, F–G) Median, 25th/75th percentiles (boxes) and Tukey range (whiskers) for the initiation rate of ligand-positive sCLSs (C, F) or ligand-positive CCPs (D, G) are shown. (E, H) Mean eGFP-CLCa fluorescence intensity grouped into CCP lifetime cohorts; error bars reflect cell-to-cell variation. The number of total CLS trajectories, CCP trajectories, and cells for each condition are (respectively): rho-EGF treated (control, DMSO): 24,737, 16,621, and 18; rho-EGF treated (BAPTA-AM treated): 33,604, 14,731, and 24; A647-Tfn (control, DMSO) 32,693, 22,008, and 24; A647-Tfn (BAPTA-AM) 35,287, 20,862, and 25. The breakdown of ligand-positive sCLSs and CCPs is as follows:  $5.0 \pm 0.7\%$  (control) and  $8.5 \pm 0.5\%$  (BAPTA-treated) of sCLSs are EGF+;  $13.2 \pm 0.9\%$  (control) and  $10.9 \pm 0.9\%$  (BAPTA-treated) of CCPs are EGF+;  $3.1 \pm 0.4\%$  (control) and  $4.0 \pm 0.7\%$  (BAPTA-treated) of sCLSs are Tfn+;  $13.6 \pm 1.9\%$  (control) and  $13.2 \pm 1.9\%$  (BAPTA-AM) of CCPs are Tfn+.

signaling to Akt phosphorylation were observed upon perturbations of cytosolic calcium (Supplemental Figure 12). The attenuation of EGFR signaling to Gab1-Akt upon perturbation of PLC $\gamma$ 1-calcium is consistent with the abrogated initiation and assembly of EGFR+ CCPs under these conditions (Figure 7, D and E).

EGFR is a member of the ErbB (HER) family of receptor tyrosine kinases and can heterodimerize with other members of this family when coexpressed, in particular HER2 (Alroy and Yarden, 1997). RPE cells do not detectably express HER2 levels, and thus EGF stimulation of these cells results in activation of EGFR homodimers (Garay et al., 2015). We have previously reported RPE cells engineered to stably express HER2 (RPE-HER2), which thus signal largely from

EGFR/HER2 heterodimers (Garay et al., 2015). Importantly, RPE-HER2 cells undergo EGF-stimulated Akt phosphorylation that is clathrin independent (Garay et al., 2015).

We next examined EGF-stimulated signaling by EGFR/HER2 heterodimers in RPE-HER2 cells to determine whether PLC $\gamma$ 1- $\text{Ca}^{2+}$  cues control EGFR signaling by control of CCPs. If so, PLC $\gamma$ 1- $\text{Ca}^{2+}$  cues would not be expected to impact signaling in RPE-HER2 cells (which signal in a clathrin-independent manner from EGFR/HER2 heterodimers). Indeed, silencing of PLC $\gamma$ 1 in RPE-HER2 cells did not impact EGF-stimulated Akt phosphorylation (Figure 9C). This suggests that, in cells lacking HER2 expression, PLC $\gamma$ 1- $\text{Ca}^{2+}$  cues control EGF-stimulated Akt phosphorylation by control of CCPs. These results indicate that PLC $\gamma$ 1- $\text{Ca}^{2+}$  signaling controls the assembly of clathrin and other proteins into EGFR+ CCPs that may thus impart upon these structures the role of signaling hubs, in addition to controlling EGFR endocytosis.

## DISCUSSION

Clathrin-mediated endocytosis controls the cell-surface abundance and initiates intracellular membrane traffic of many proteins, and thus has key roles in the control of nutrient and ion transport, cell adhesion, and receptor signaling (McMahon and Boucrot, 2011; Antonescu et al., 2014). Clathrin-mediated endocytosis controls the internalization of many different membrane proteins, each which may require unique regulation. It is thus important to resolve how the clathrin-mediated endocytosis of different membrane proteins can be distinctly controlled.

Using multiple independent approaches, including siRNA silencing of PLC $\gamma$ 1, pharmacological antagonism of IP3R, and chelation of cytosolic  $\text{Ca}^{2+}$ , we identified that PLC $\gamma$ 1-derived, IP3-dependent  $\text{Ca}^{2+}$  signaling is required for the clathrin-mediated endocytosis of EGFR but not of other receptors such as Tfr. While it is possible that each of these approaches has off-target effects, the strikingly similar phenotype of each perturbation to selectively impair the clathrin-mediated

internalization of EGFR strongly indicates that the effect of each is specific to perturbation of PLC $\gamma$ 1-derived IP3-dependent  $\text{Ca}^{2+}$  signaling. Consistent with the distinct control of the clathrin-mediated endocytosis of EGFR (but not that of Tfr) by these  $\text{Ca}^{2+}$  signals, we found that EGFR and Tfr reside largely in distinct clathrin structures at the cell surface. Perturbation of intracellular  $\text{Ca}^{2+}$  selectively impaired the earliest stages of initiation and assembly of CCPs harboring EGFR. Notably,  $\text{Ca}^{2+}$  signaling controlled the recruitment of certain proteins, such as Sjn1 and clathrin, to CCPs. Finally, perturbation of PLC $\gamma$ 1 and  $\text{Ca}^{2+}$  impaired the clathrin-dependent activation of Akt signaling by EGFR, suggesting that  $\text{Ca}^{2+}$  signals control both clathrin-dependent EGFR signaling and endocytosis.

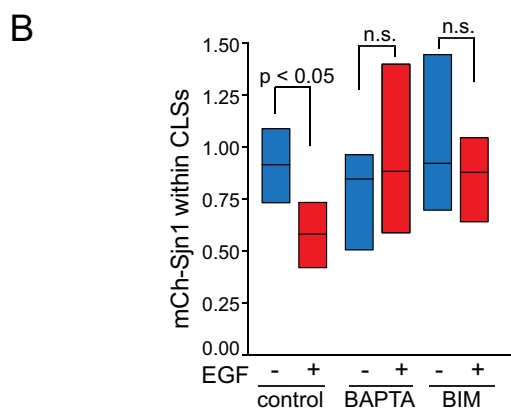
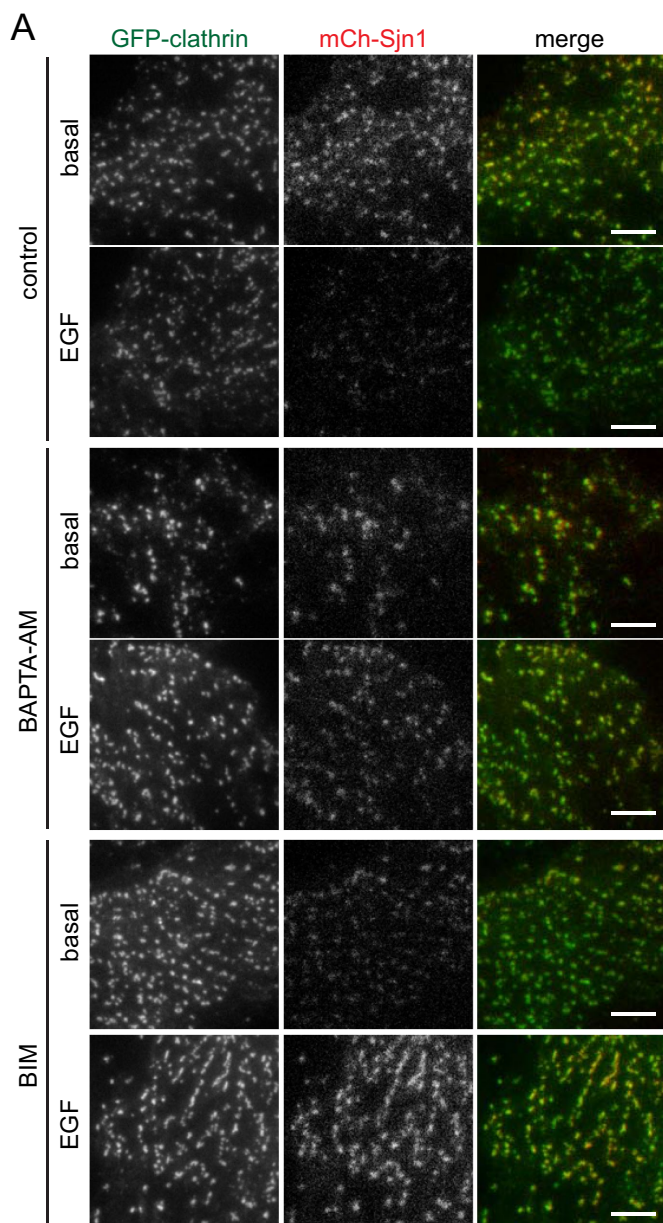


**FIGURE 8:** mCherry-Sjn1 is depleted from CLSs upon EGF stimulation in a  $Ca^{2+}$ - and PKC-dependent manner. RPE cells stably expressing GFP-CLCa were transfected with mCherry-tagged Sjn1 (mCh-Sjn1, 170-kDa isoform), and then treated with 10  $\mu$ M BAPTA-AM for 15 min, 1  $\mu$ M BIM for 30 min, or left untreated (control), followed in some samples by stimulation with 5 ng/ml EGF, as indicated, then

### Regulation of CCPs and clathrin-mediated endocytosis by intracellular calcium

The regulation of clathrin-mediated endocytosis by  $Ca^{2+}$  has been appreciated for some time in presynaptic neurons. Membrane depolarization triggers robust  $Ca^{2+}$ -dependent exocytosis of synaptic vesicles, which is coupled to enhanced clathrin-mediated endocytosis (Saheki and De Camilli, 2012). This increase in intracellular  $Ca^{2+}$  during depolarization is thought to contribute to enhanced clathrin-mediated endocytosis in neurons, at least in part due to calcineurin-dependent dephosphorylation of Sjn1, dynamin1, amphiphysins, Eps15, and endophilin (Liu *et al.*, 1994; Bauerfeind *et al.*, 1997; Slepnev *et al.*, 1998; Chen *et al.*, 1999; Cousin *et al.*, 2001).

Here we reveal that  $Ca^{2+}$  signals also control clathrin-mediated endocytosis in nonneuronal cells and that these signals are selectively required for EGFR endocytosis. Moreover, calcineurin and dynamin1 were dispensable for the internalization of EGFR (Figure 4A and Supplemental Figure 3, A and B), suggesting that  $Ca^{2+}$ -dependent control of clathrin-mediated endocytosis in RPE cells does not rely on acute dephosphorylation of endocytic proteins such as dynamin1 by calcineurin, a phenomenon that regulates the clathrin-mediated endocytosis of TRAIL/DR (Reis *et al.*, 2017). Given that the control of endocytosis by  $Ca^{2+}$  in RPE cells is at least partly distinct from that thought to occur in neurons, how may calcium signals control clathrin-mediated endocytosis of EGFR in nonneuronal cells?

The regulation of clathrin-mediated endocytosis of EGFR by  $Ca^{2+}$ -derived signals does not prevent the nucleation of EGFR+ clathrin structures, as observed with the increase in EGF+ sCLSs (Figure 7C), yet impacts the subsequent initiation and assembly of bona fide CCPs harboring EGFR (Figure 7D). Both sCLSs and CCPs represent nucleation of clathrin structures (Aguet *et al.*, 2013; Mettlen and Danuser, 2014; Kadlecova *et al.*, 2017). Interestingly, mutation of the cargo-binding motifs of AP2 reduces the initiation rate of both sCLSs and bona fide CCPs, measured by methods similar to those used here (Kadlecova *et al.*, 2017), indicating that cargo recruitment to clathrin structures contributes to clathrin-structure nucleation. Indeed, perturbation of  $Ca^{2+}$  signals does not impair the total recruitment of EGFR to CLSs (Figure 6C), of which a large fraction are sCLSs that do not give rise to bona fide CCPs (Aguet *et al.*, 2013). This suggests that  $Ca^{2+}$  signals do not control EGFR activation or recruitment to nascent clathrin nucleations. Instead,  $Ca^{2+}$  signals control the subsequent initiation of bona fide CCPs harboring EGFR from nascent clathrin nucleations (Figure 7D) and the recruitment of clathrin (Figure 7E), Sjn1 (Figure 8 and Supplemental Figure 11), and perhaps other proteins.

Sjn1 recruitment to CCPs is regulated by  $Ca^{2+}$  signals and PKC (Figure 8 and Supplemental Figures 10 and 11). Sjn1 has two

by immediate fixation. (A) Shown are representative micrographs obtained by TIRF-M. Scale bars: 10  $\mu$ m. Full-image panels, including corresponding epifluorescence images, are shown in Supplemental Figure 10. (B) TIRF-M images were subjected to automated detection of CLSs, followed by quantification of the mean mCh-Sjn1 fluorescence intensity therein (normalized to total mCh-Sjn1 expression determined from epifluorescence images). Shown in B are median (bar) and 25th/75th percentiles (boxes) of mCh-Sjn1 fluorescence intensity within CLSs in each condition. The number of CLSs and cells analyzed, respectively, for each condition are as follows: basal, control (no drug): 43,047 and 50; basal, BAPTA-AM: 38,919 and 44; basal, BIM: 35,556 and 46; EGF, control (no drug): 55,482 and 55; EGF, BAPTA-AM: 28,644 and 43; EGF, BIM: 29,637 and 38; from three independent experiments.

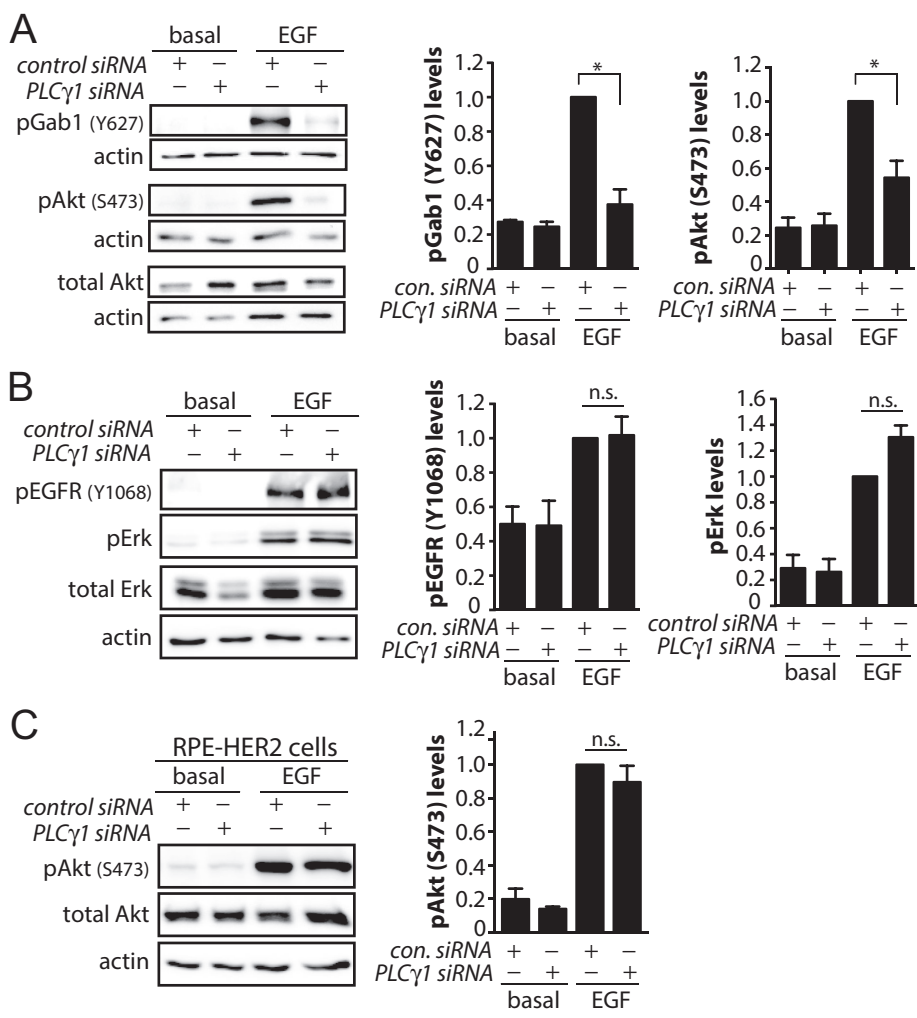


**FIGURE 9:** PLCγ1 is required for clathrin-dependent EGFR signaling. RPE cells or RPE cells stably expressing HER2 (RPE-HER2 cells) were subjected to siRNA silencing of PLCγ1 and treated with 5 ng/ml EGF for 5 min as indicated, followed by Western blotting of whole-cell lysates with antibodies to detect phosphorylated proteins. Shown are representative immunoblots and the mean ± SE signal intensity for (A) pAkt and pGab1 in RPE cells (not expressing HER2), (B) pEGFR and pErk in RPE cells (not expressing HER2), and (C) pAkt in RPE-HER2 cells. \*,  $p < 0.05$ .

isoforms, a neuronal-enriched 145-kDa isoform and a ubiquitous 170-kDa isoform (McPherson et al., 1996; Ramjaun and McPherson, 1996). Both Sjn1-145 and -170 have NPF and PRD domains that interact with Eps15 and endophilin, while Sjn1-170 also interacts with AP2 and clathrin (Perera et al., 2006). While both isoforms are recruited to CCPs, Sjn1-145 is largely recruited near the end of the lifetime of a CCP, while Sjn1-170 is recruited along with clathrin and AP2 and is present throughout the lifetime of CCPs (Perera et al., 2006; Antonescu et al., 2011). Sjn1 has 5-phosphatase and Sac1 domains important for the conversion of PIP2 to phosphatidylinositol-4-phosphate and phosphatidylinositol, a process critical for uncoating of clathrin-coated vesicles once internalized (Cremona et al., 1999). Further, due to recruitment at early stages of clathrin-structure formation, Sjn1 also negatively regulates the stabilization of nascent clathrin structures in a manner that requires the 5-phosphatase domain (Antonescu et al., 2011). Hence the turnover of PIP2 by Sjn1 within nascent CCPs impairs CCP formation. As such, the EGF-stimulated reduction in Sjn1 recruitment to CCPs may increase CCP initiation and efficiency of CCP internalization, thus promoting EGFR endocytosis. Notably, it appears that EGF stimulation elicits a broad

depletion of Sjn1 from the majority of visible CCPs (Figure 8A and Supplemental Figure 11A), suggesting that depletion of Sjn1 is not restricted to EGF+ clathrin structures. As Sjn1 silencing impacted CCP dynamics but not Tfn internalization (Antonescu et al., 2011), we conclude that clathrin structures harboring EGFR are more sensitive to the regulation of Sjn1 recruitment than those harboring TfR.

EGF stimulation may reduce Sjn1 recruitment to CCPs by direct regulation of Sjn1 or by broader reprogramming of CCP assembly. Consistent with the former, Sjn1 can undergo tyrosine phosphorylation by the EphB receptor (Irie et al., 2005) or serine phosphorylation by CDK5 (Lee et al., 2004), modifications that each control the interaction of Sjn1 with endophilin and/or its phosphatase activity. Notably, PKC may also mediate Sjn1 phosphorylation in nerve terminals (Cousin et al., 2001).

Ca<sup>2+</sup> and PKC may also more broadly control CCP assembly and clathrin-mediated endocytosis. Ca<sup>2+</sup> may control endocytosis by direct binding to clathrin light chain (Mooibroek et al., 1987; Nathke et al., 1990) or by regulation of annexin 2 and 6, which control AP2 recruitment to membranes (Creutz and Snyder, 2005; Cornely et al., 2011). The control of endocytosis by calcium may also occur in yeast, as the N-BAR domain protein Rvs167 is regulated by calmodulin, impacting release of vesicles from the membrane (Myers et al., 2016). Our findings that Ca<sup>2+</sup> signals control the assembly and size of certain CCPs is consistent with the glucose-induced enhanced endocytosis in INS-1 cells (MacDonald et al., 2005). While clathrin assembly or clathrin-mediated endocytosis was not directly examined, the glucose-induced Ca<sup>2+</sup> signals in

INS-1 cells enhance endocytosis and control the size of endocytic vesicles. While we show here that PKC is required for regulation of clathrin-mediated endocytosis of EGFR, a previous study concluded that PKC regulated EGFR recycling but not internalization (Bao et al., 2000). This study examined the effect of treatment of cells with phorbol 12-myristate 13-acetate (PMA, which results in broad activation of PKC), which did not impact EGF internalization. Our observations indicate that EGF-elicited Ca<sup>2+</sup> signals are sufficient to activate PKC to regulate EGFR internalization in the absence of PMA treatment.

Given the complexity and heterogeneity of CCPs, including their lifetime and composition, dissecting the mechanism by which Ca<sup>2+</sup> and PKC signals control CCP assembly, maturation, and scission from the cell surface is beyond the scope of this study and represents an important area of investigation for future research. Importantly, we establish that PLCγ1-derived Ca<sup>2+</sup> and PKC signals control the clathrin-mediated endocytosis of EGFR as a result of regulation of initiation and assembly of bona fide EGFR+ CCPs.

Interestingly, while this article was under review, Sigismund and colleagues reported that PLC-derived Ca<sup>2+</sup> signals control

nonclathrin endocytosis (NCE) of EGFR (Caldieri *et al.*, 2017), which occurs in some cells upon stimulation with high doses of EGF (>20–50 ng/ml) (Sigismund *et al.*, 2008). Nonetheless, our work establishes that PLC $\gamma$ 1 and Ca $^{2+}$  control clathrin-mediated endocytosis of EGFR as 1) EGF internalization is very largely clathrin dependent in RPE cells (Garay *et al.*, 2015), even at high (100 ng/ml) doses of EGFR (Supplemental Figure 2A); 2) direct observation of clathrin structures and CCP dynamics resolves the question of whether Ca $^{2+}$  signals control CCP initiation and assembly (Figures 6 and 7); and 3) Ca $^{2+}$  signals are shown to control the recruitment of specific proteins (Sjn1) into CCPs (Figure 8 and Supplemental Figures 10 and 11). Taken together, these studies suggest that Ca $^{2+}$  signals may represent a broad, common regulator of EGFR internalization through multiple endocytic pathways.

### Distinct regulation of clathrin-mediated endocytosis of EGFR versus Tfr

Several lines of evidence support the internalization of EGFR and Tfr through largely distinct CCPs. Silencing of AP2 subunit components (Motley *et al.*, 2003) or sequestration of AP2 by overexpression of AAK1 (Conner and Schmid, 2003) results in near-complete impairment of Tfr endocytosis, with minimal effect on clathrin-mediated endocytosis of EGFR. However, others have reported complete inhibition of both Tfr and EGFR endocytosis upon AP2 silencing (Huang *et al.*, 2004; Rappoport and Simon, 2009), and AP2 is found in virtually all CCPs (Keyel *et al.*, 2006). Taken together, these studies suggest that AP2 may be required for internalization of both Tfr and EGFR but that the endocytosis of each receptor may use AP2 in a functionally distinct manner under some contexts. Furthermore, phosphatidic acid controls CCP dynamics but impacts only the clathrin-mediated endocytosis of EGFR, not Tfr (Antonescu *et al.*, 2010).

Here we employed labeling of Tfr and EGFR using fluorescently conjugated ligands coupled to automated and unbiased image analysis to resolve that these two receptors are localized largely within distinct CCPs (Figure 5). We find that CCPs harboring either significant levels of EGFR or Tfr (but not both) are detected approximately three times as frequently as CCPs that harbor both receptors. This relationship was not altered by increasing the levels of fluorescently labeled EGF used for stimulation in this experiment (Figure 5C). Thus incomplete labeling of Tfr or EGFR by labeling with their respective fluorescent ligands does not readily explain the observed enrichment of EGFR and Tfr into largely distinct CCPs. Instead, these observations suggest that EGFR and Tfr, and not just their ligands, are recruited to largely separate sets of CCPs.

Most CCPs that are positive for Tfr contain multiple copies of this receptor, including when labeled using an exofacial synthetic ligand that is comparable in size to fluorescent Tfn (and thus also much larger than fluorescent EGF) (Tosoni *et al.*, 2005; Liu *et al.*, 2010). Thus it is very unlikely that our observation of fluorescent EGF and Tfn enrichment within distinct CCPs is due to steric constraints limiting the inclusion of multiple ligands into the same clathrin structure. Indeed examination of the EGF and Tfn intensity distribution in CCPs (Figure 5B) reveals that a range of ligand fluorescence intensities within CCPs exists for each receptor ligand, indicating that many CCPs have more than one of their respective ligands (EGF or Tfn).

The recruitment of EGFR and Tfr to largely distinct CCPs is consistent with some previous studies. These two ligands were observed in largely distinct CCPs with methods similar to those we employed here relying on fluorescently conjugated Tfn and EGF coupled to TIRF-M, (Tosoni *et al.*, 2005). While CCPs harboring both EGF and Tfr can indeed be detected by electron microscopy (Lamaze *et al.*, 1993), labeling of EGFR and Tfr using antibodies

specific for each receptor and immunoelectron microscopy revealed that these receptors were far more frequently detected within distinct CCPs than in the same CCPs (Tosoni *et al.*, 2005). And consistently, while CCPs were not being examined directly, fluorescent EGF and Tfn were shown to exhibit reduced overlap in the initial stages of internalization (Leonard *et al.*, 2008). These studies support our conclusion, based on systematic and unbiased analysis of CCPs, that EGFR and Tfr are largely found in distinct CCPs.

The recruitment of EGFR and Tfr to largely distinct CCPs may occur as a result of stochastic recruitment of receptors to preformed early clathrin structures that are intrinsically capable of interaction with and subsequent internalization of diverse cargo receptors. Alternatively, the selective incorporation of EGFR into CCPs that have unique properties compared with CCPs harboring Tfr suggests that a deterministic cargo-selection mechanism may gate the early stages of clathrin-structure nucleation, initiation, and assembly. Consistent with this interpretation, EGF stimulation of AP2 silenced cells resulted in the formation of CCPs that contained EGF, EGFR, and clathrin but not Tfr (Johannessen *et al.*, 2006). If the stochastic segregation of receptors into largely distinct CCPs predominates, then this phenomenon may be subject to cell context-specific parameters, such as receptor expression levels.

Regardless, EGFR and Tfr reside largely within distinct clathrin structures in RPE cells. This cargo segregation is likely not restricted to RPE cells, as similar findings were observed in HeLa cells (Tosoni *et al.*, 2005). Notably, the incorporation of cargo within specific CCPs alters the properties of those CCPs, as shown for low-density lipoprotein receptor (Mettlen *et al.*, 2010) and certain GPCRs (Puthenveedu and von Zastrow, 2006). These studies suggest that the recruitment of each receptor to particular clathrin structures may be coupled to unique engagement of endocytic accessory proteins that impact CCP formation, assembly, maturation, and scission. As such, CCPs harboring EGFR are dependent on contributions from PLC $\gamma$ 1-derived Ca $^{2+}$  signals for CCP initiation and assembly and eventual productive formation of intracellular vesicles. In contrast, CCPs harboring Tfr are not regulated by PLC $\gamma$ 1-derived Ca $^{2+}$  signals.

### Regulation of EGF-stimulated Akt phosphorylation by PLC $\gamma$ 1-derived signals

We recently uncovered that clathrin structures, but not receptor endocytosis, are required for EGFR signaling leading to Gab1 and Akt phosphorylation (Delos Santos *et al.*, 2015; Garay *et al.*, 2015; Lucarelli *et al.*, 2016). Perturbations of clathrin selectively impaired EGF-stimulated phosphorylation of Gab1 and Akt, but were without effect on phosphorylation of EGFR or of other signaling pathways such as mitogen-activated protein kinase (MAPK). Importantly, perturbations of dynamin2, which allowed formation of CCPs and recruitment of EGFR therein, but not receptor internalization into vesicles, did not impair EGF-stimulated Akt phosphorylation. We proposed that in addition to forming endocytic portals, a subset of clathrin structures also function as signaling microdomains, required for the enrichment of specific receptor signals. Consistent with this, we observed the enrichment of phosphorylated Gab1 within CCPs upon stimulation with ligands of EGFR or Met (Garay *et al.*, 2015; Lucarelli *et al.*, 2016).

Here we find that PLC $\gamma$ 1 and intracellular Ca $^{2+}$  are required for EGF-stimulated activation of clathrin-dependent signals (phosphorylation of Gab1 and Akt) but not clathrin-independent signals (phosphorylation of EGFR and MAPK). Given that PLC $\gamma$ 1 and intracellular Ca $^{2+}$  control assembly of CCPs harboring EGFR, we propose that these signals are also required to prime clathrin structures to function as signaling microdomains required for Akt activation.

The requirement for PLC $\gamma$ 1 for EGF-stimulated Akt phosphorylation may reflect the requirement for PLC $\gamma$ 1 and Ca<sup>2+</sup> in the initiation and assembly of EGFR+ clathrin structures, which are required for signaling leading to Akt activation, or other mechanism(s). We observed that EGF-stimulated Akt phosphorylation in RPE cells engineered to stably express HER2 (which signal largely from EGFR/HER2 heterodimers) does not require PLC $\gamma$ 1 for EGF-stimulated Akt phosphorylation (Figure 9C). Because clathrin is dispensable for EGF-stimulated Akt phosphorylation in RPE-HER2 cells (Garay *et al.*, 2015), the requirement for PLC $\gamma$ 1 for activation of Akt by EGFR may be limited to cellular contexts in which EGFR signaling is clathrin dependent. This result strengthens our conclusion that PLC $\gamma$ 1 and Ca<sup>2+</sup>-dependent signals regulate clathrin-mediated endocytosis of EGFR, as well as clathrin-dependent EGFR signaling. The largely unaltered EGF-stimulated Akt phosphorylation observed in PLC $\gamma$ 1<sup>-/-</sup>MEFs (Ji *et al.*, 1998) may thus reflect a different cellular context (e.g., HER2 coexpression) in which EGF-stimulated Akt phosphorylation occurs in a clathrin-independent manner or another long-term adaptation to PLC $\gamma$ 1 genetic knockout.

We thus conclude that the regulation of signaling and endocytosis of EGFR is reciprocal, as the regulation of CCP initiation and assembly by EGF-stimulated PLC $\gamma$ 1-Ca<sup>2+</sup> signals in turn control EGF-stimulated Akt signaling. Elucidating the mechanisms by which clathrin structures may integrate a number of intracellular cues, which in turn regulate signaling by EGFR and other cell-surface receptors, should be the subject of future research in the function and regulation of CCPs.

In summary, we reveal an unprecedented dimension by which functionally distinct subsets of CCPs can be differently regulated by diffusible signals (e.g., Ca<sup>2+</sup>) (Supplemental Figure 13). The specific and distinct regulation of subsets of CCPs by cellular signals provides the basis for how the versatile assembly of CCPs can be modulated to accomplish distinct regulation of the diverse proteins of the cell-surface proteome.

## MATERIALS AND METHODS

### Materials

DMEM/F12, fetal bovine serum (FBS), penicillin/streptomycin solution, insulin-Tfn-selenium-ethanolamine solution, and sterile HEPES buffer were obtained from Life Technologies (Carlsbad, CA). L-Glutamine was obtained from Sigma-Aldrich (St. Louis, MO). Human EGF (unlabeled), EGF (complexed to Alexa Fluor 555 [A555-EGF] or rhodamine [rhodamine-EGF]), Tfn (complexed to Alexa Fluor 555 [A555-Tfn] or Alexa Fluor 647 [A647-Tfn]), biotin-xx-EGF, and biotin-xx-Tfn were obtained from Life Technologies (Carlsbad, CA). Anti-EGF antibodies (used in EGF uptake assay) were from Upstate Biotechnologies (Millipore, Etobicoke, ON, Canada), and Tfn-antibodies (used in Tfn uptake assay) were from Bethyl Laboratories (Montgomery, TX). Avidin and o-phenylenediamine hydrochloride reagent were obtained from Biobasic (Markham, ON, Canada), and biocytin was obtained from Santa Cruz Biotechnology (Dallas, TX). Superblock blocking buffer was obtained from Thermo Fisher (Rockford, IL).

BIM and CsA were obtained from Cell Signaling (Danvers, MA), XeC was obtained from Abcam (Cambridge, MA), and BAPTA-AM was obtained from Santa Cruz Biotechnology (Dallas, TX).

Antibodies used for immunofluorescence to detect Sjn1 were from Synaptic Systems (Goettingen, Germany), and anti-AP2 (Abcam) and antibodies used for Western blotting were obtained as follows: for detection of phospho-Akt (pS473) from Life Technologies (Carlsbad, CA), and for total Akt, phospho-Erk, total Erk, phospho-EGFR, phospho-PLC $\gamma$ 1, total PLC $\gamma$ 1, and actin from Cell Signaling (Danvers, MA).

cDNA constructs encoding the wild-type pleckstrin homology (PH) domain of PLC $\delta$ 1 fused to mCherry (mCherry-PH WT) or of the PH domain harboring K32A W36A mutations to abolish binding to PIP2 similarly fused to mCherry were previously described (Antonescu *et al.*, 2011). cDNA encoding Sjn1 (170-kDa isoform) fused to mCherry was previously described (Antonescu *et al.*, 2011). Hemagglutinin (HA)-NFAT1(4-460)-GFP was a gift from Anjana Rao, Harvard Medical School (Addgene plasmid #11107) (Aramburu *et al.*, 1999). siRNA sequences used were as follows (sense): dynamin1, 5'-GGCUUA-CAUGAACACCAACCACGAA (Reis *et al.*, 2015); clathrin heavy chain (CHC), GGAAGGAAUUGCAGAAGAAUU (Garay *et al.*, 2015); PLC $\gamma$ 1, GAGCAGUGCCUUUGAAGAAUU; or nontargeting control siRNA, CGUACUGCUUGCGAUACGGUU; and were obtained from Dharmacon (Lafayette, CO) or Sigma-Aldrich (St. Louis, MO).

### Cell culture, transfection, and drug treatments

Wild-type ARPE-19 (RPE herein) human retinal pigment epithelial cells (RPE-WT) and derivative lines stably expressing clathrin light chain fused to eGFP (RPE eGFP-CLC) or Tag-RFP-T (RPE RFP-CLC) were used as previously described (Antonescu *et al.*, 2011; Aguet *et al.*, 2013). Cells were cultured in DMEM/F12 supplemented with 10% FBS, 100 U/ml penicillin, and 100  $\mu$ g/ml streptomycin at 37°C and 5% CO<sub>2</sub>. RPE cells engineered to stably express HER2 (RPE-HER2) were previously described, and cultured similarly as RPE-WT cells, with the addition of 1  $\mu$ g/ml puromycin to growth medium (Garay *et al.*, 2015).

### cDNA and siRNA transfection

cDNA transfection (as per Figures 2 and 8 and Supplemental Figures 3 and 10) was performed using Lipofectamine 2000 (Life Technologies, Carlsbad, CA), as per the manufacturer's instructions and as previously described (Garay *et al.*, 2015; Bone *et al.*, 2017). Briefly, for each well of a six-well plate, 2.5  $\mu$ g of cDNA was precomplexed with 5  $\mu$ l of transfection reagent in Opti-MEM. Cells were subsequently incubated with DNA-reagent complexes for 4 h, followed by washing and incubation of cells in regular growth medium for 18–24 h before the start of the experiment.

siRNA gene silencing (as per Figures 1, 2, and 9 and Supplemental Figures 1–3) was performed using Lipofectamine RNAiMAX (Life Technologies, Carlsbad, CA), as per the manufacturer's instructions and as previously described (Garay *et al.*, 2015; Ross *et al.*, 2015). Briefly, each siRNA construct was transfected at 220 pmol/l precomplexed to the transfection reagent in Opti-MEM for 4 h, after which cells were washed and replaced in regular growth medium. siRNA transfections were performed twice (72 h and 48 h) before each experiment.

### Inhibitor treatment and EGF stimulation

For all experiments, cells were subjected to serum starvation for 1 h before the start of the assay. Following serum starvation, cells were treated with small-molecule pharmacological inhibitors as follows: 1  $\mu$ M BIM for 30 min (Wijesekara *et al.*, 2006), 3  $\mu$ M XeC for 30 min (Miyamoto *et al.*, 2000), 10  $\mu$ M CsA for 30 min, or 10  $\mu$ M BAPTA-AM for 15 min, or treated in media containing a corresponding volume of vehicle (dimethyl sulfoxide [DMSO]), in each case <0.1%, control condition).

All experiments were performed with EGF stimulation at 5 ng/ml unless otherwise stated.

### TIRF-M measurement of cell-surface PIP2 abundance

RPE cells were seeded onto glass coverslips and transfected with nontargeting siRNA, then with cDNA encoding either the wild-type

PH domain of PLC $\delta$ 1 fused to mCherry (mCherry-PH WT) or of the PH domain harboring K32A and W36A mutations to abolish binding to PIP2 similarly fused to mCherry (mCherry-PH K32A, W36A). On the day of the experiment, cells were serum starved for 1 h, then treated with 5 ng/ml EGF for 5 min, followed by immediate fixation in 4% paraformaldehyde (PFA). Cells were then imaged using sequential TIRF-M and wide-field epifluorescence microscopy using a 150 $\times$ /1.45 NA objective on an Olympus IX81 instrument equipped with CellTIRF modules (Olympus Canada, Richmond Hill, ON, Canada) using 561-nm (50 mW) laser illumination and an 624/50 emission filter. Images were acquired using a C9100-13 EM-CCD camera (Hamamatsu, Bridgewater, NJ).

Images were analyzed using ImageJ (Schneider *et al.*, 2012) by manually delineating a region of interest corresponding to the cell outline, followed by measurement of the mean pixel intensity within this region (Ross *et al.*, 2015) for each of the TIRF-M and epifluorescence channels for each cell. To obtain the relative cell-surface localization index for the mCherry-PH probes under various conditions, we determined the ratio of TIRF/epifluorescence for each cell. Measurements were subjected to analysis of variance (ANOVA) followed by Tukey's posttest, with a threshold of  $p < 0.05$  for statistically significant differences between conditions (Figure 2B).

### Biochemical measurement of phosphoinositide levels

RPE cells were incubated for 24 h in inositol-free DMEM (MP Biomedicals, Santa Ana, CA) with 10 Ci/ml *myo*-[2-3 H(N)] inositol (PerkinElmer Life Sciences, Waltham, MA), 10% FBS, 4 mM L-glutamine, 1 $\times$  insulin-Tfn-selenium-ethanolamine 20 mM HEPES, and 1 $\times$  penicillin/streptomycin. On the day of the experiment, cells were serum starved for 1 h and then stimulated with 5 or 20 ng/ml EGF for 5 min or with 10  $\mu$ M ionomycin for 20 min, as indicated. Cells were then treated with 600  $\mu$ l of 4.5% perchloric acid (vol/vol) on ice for 15 min, scraped, and pelleted at 12,000  $\times$  g for 10 min. Pellets were washed with 1 ml ice-cold 0.1 M EDTA and resuspended in 50  $\mu$ l of water. Phospholipids were deacylated with 500  $\mu$ l of a solution of methanol/40% methylamine/1-butanol (45.7% methanol:10.7% methylamine:11.4% 1-butanol [vol/vol]) for 50 min at 53 $^{\circ}$ C. Samples were vacuum-dried and washed twice with water. The dried samples were then resuspended in water, extracted with a solution of 1-butanol/ethyl ether/ethyl formate (20:4:1), vortexed for 5 min, and centrifuged at 12,000  $\times$  g for 2 min. The bottom aqueous layer was collected and extracted twice more. The aqueous layer was vacuum-dried and resuspended in 50  $\mu$ l of water. Equal counts of  $^3$ H were separated by high-performance liquid chromatography (Agilent Technologies, Santa Clara, CA) through an anion exchange 4.6  $\times$  250 mm column (Phenomenex, Torrance, CA) with a flow rate of 1 ml/min and subjected to a gradient of water (buffer A) and 1 M (NH $_4$ ) $_2$ HPO $_4$ , pH 3.8 (buffer B) as follows: 0% B for 5 min, 0–2% B for 15 min, 2% B for 80 min, 2–10% B for 20 min, 10% B for 30 min, 10–80% B for 10 min, 80% B for 5 min, and 80–0% B for 5 min. The radiolabeled eluate was detected by  $\beta$ -RAM 4 (LabLogic, Brandon, FL) with a 1:25 ratio of eluate to scintillant (LabLogic) and analyzed using Laura 4 software. Each of the phosphoinositides was normalized against the parent phosphatidylinositol peak. Samples were subjected to ANOVA followed by Tukey's posttest, with a threshold of  $p < 0.05$  for statistically significant differences between conditions (Figure 2A).

### EGF and Tfn ligand internalization assays

All internalization assays were performed on RPE-WT cells grown on 12-well plates as previously described (Garay *et al.*, 2015). Following

siRNA gene silencing (Figure 1 and Supplemental Figures 2 and 3) or drug treatments (Figures 2 and 3), cells were then incubated with either biotin-xx-EGF (5 ng/ml for EGF internalization) or biotin-xx-Tfn (1  $\mu$ g/ml for Tfn internalization) for 0, 2, 5, or 10 min at 37 $^{\circ}$ C. Following ligand internalization, cells were immediately placed on ice and washed three times in ice-cold PBS $^{2+}$  (phosphate-buffered saline [PBS] supplemented with 1 mM CaCl $_2$  and 1 mM MgCl $_2$ ) to remove unbound ligand and arrest membrane traffic. Bound, uninternalized ligands were subsequently quenched by sequential incubation with free avidin for 30 min on ice (for EGF internalization at 5  $\mu$ g/ml avidin, and for Tfn internalization at 28.6  $\mu$ g/ml) and biocytin for 15 min on ice (for EGF internalization with 7.69  $\mu$ g/ml biocytin, and for Tfn internalization with 27.3  $\mu$ g/ml). Subsequently cells were washed repeatedly with ice-cold PBS $^{2+}$  and solubilized by incubation in a buffer composed of 0.01% Triton X-100 and 0.01% SDS in Superblock. Cell lysates were then plated onto enzyme-linked immunosorbent assay (ELISA) plates coated with either anti-EGF or anti-Tfn antibodies, followed by detection of biotin-xx-EGF or biotin-xx-Tfn (free, unbound to avidin) by incubation with streptavidin conjugated to horseradish peroxidase (POD), and detection of bound POD by o-phenylenediamine assay. Absorbance readings corresponding to internalized biotin-xx-EGF or biotin-xx-Tfn readings were then normalized to the total levels of surface-ligand binding measured at 4 $^{\circ}$ C and not subjected to avidin-biocytin quenching, performed in parallel for each condition.

To resolve whether any differences in EGF internalization observed using the above assay might be due to changes in EGF:EGFR binding (instead of EGF:EGFR internalization rate), we performed a control experiment to measure cell-associated biotin-xx-EGF (reflecting EGF:EGFR binding) in which the quenching by avidin and biocytin was omitted (Supplemental Figure 2B). This assay was performed identically to the above EGF internalization assay, with the exception that, following ligand internalization (at 37 $^{\circ}$ C), placement of cell on ice, and extensive washing in ice-cold PBS $^{2+}$  to remove unbound ligand, cells were directly solubilized by incubation 0.01% Triton X-100 and 0.01% SDS in Superblock buffer. Cell-associated biotin-xx-EGF was detected on EGF-coated ELISA plates, as described above, and normalized to total biotin-xx-EGF bound (at 4 $^{\circ}$ C).

Measurement of biotin-xx-Tfn internalization during EGF stimulation was performed similarly as Tfn internalization described above, but was preceded by the addition of 5 ng/ml EGF (unlabeled) 1 min before addition of Tfn-xx-biotin in each sample. Measurement of Tfn-xx-biotin was performed in the continued presence of unlabeled EGF.

In all EGF or Tfn internalization experiments, the results were subjected to two-way ANOVA followed by Bonferroni's multiple comparison posttest, with a threshold of  $p < 0.05$  for significant difference between treatment conditions.

### Measurement of cytosolic [Ca $^{2+}$ ] with Fluo4-AM

RPE-WT cells were seeded onto glass coverslips and then subjected to siRNA silencing as described earlier. At the time of the experiment, cells were loaded with 8  $\mu$ M Fluo-4 AM for 15 min at 37 $^{\circ}$ C and 5% CO $_2$ ; this was followed by washing to remove excess Fluo-4 AM and a further 30 min incubation at 37 $^{\circ}$ C and 5% CO $_2$ , during which time some cells were treated with XeC, as indicated. Spinning-disk confocal microscopy of living cells was performed at 37 $^{\circ}$ C and 5% CO $_2$  throughout image acquisition using an Olympus IX81 equipped with a Yokogawa CSU X1 scanhead and a 60 $\times$ /1.35 NA oil objective using a Hamamatsu C9100-13 EM-CCD camera. Excitation light was provided by 488 nm (100 mV) laser illumination, and emitted light was collected following passage through a 525/50 emission filter.

Images of multiple fields of view of unstimulated cells (basal) were obtained, followed by addition of 5 ng/ml EGF for 5 min and acquisition of images of multiple fields of view of the EGF-stimulated condition. For testing the maximum intensity of Fluo4-AM fluorescence, subsequent to EGF stimulation, cells were treated with 10  $\mu$ M ionomycin for 5 min at 37°C in the presence of 5% CO<sub>2</sub>, followed by acquisition of images of multiple fields of view of the ionomycin-treated condition. All images were analyzed using ImageJ, measuring the total intensity of Fluo4-AM per cell in each condition (before EGF, after EGF, and after ionomycin). Shown in Figure 2, D, F, and G, are the differences in the mean Fluo4-AM fluorescence between the EGF-stimulated and basal conditions and the differences in the mean Fluo4-AM fluorescence between the ionomycin-treated and EGF-stimulated conditions. The results were subjected to one-way ANOVA followed by Tukey's posttest, with a threshold of  $p < 0.05$  for statistically significant differences between conditions.

### **TIRF and spinning-disk confocal microscopy and automated image analysis of CLSs (fixed cells)**

**Fixed sample preparation for CLS detection and analysis by TIRF-M.** RPE cells stably expressing eGFP-CLC were seeded onto glass coverslips the day before the experiment, and in some cases transfected with cDNA encoding mCherry-Sjn1-170 (Figure 8 and Supplemental Figure 10). Following 1-h serum starvation and drug treatment as indicated, cells were treated with 20 ng/ml rhodamine EGF and 10  $\mu$ g/ml A657-Tfn (alone or in combination) (Figure 5), either 5 ng/ml A555-EGF or 5  $\mu$ g/ml A555-Tfn for 3 min (Figure 6), or unlabeled EGF (Figure 8 and Supplemental Figure 10) followed by immediate fixation in 4% PFA. For experiments shown in Supplemental Figure 11, endogenous Sjn1 was labeled by immunofluorescence staining as previously described (Garay et al., 2015), using anti-Sjn1 antibodies.

**Fixed sample preparation for CCP detection and analysis by spinning-disk confocal microscopy.** Parental RPE cells (not expressing any fluorescent protein) were treated with 20 ng/ml rhodamine EGF and 10  $\mu$ g/ml A657-Tfn (alone or in combination), followed by immediate fixation in 4% PFA and immunostaining with anti-AP2 specific antibodies.

**Image acquisition by TIRF-M and spinning-disk confocal microscopy.** For experiments shown in Figure 6 and Supplemental Figures 7 and 11, samples were imaged by TIRF-M using a 150 $\times$ /1.45 NA objective on an Olympus IX81 instrument equipped with CellTIRF modules (Olympus Canada, Richmond Hill, ON, Canada) using 491- and 561-nm laser illumination and 520/30 and 624/50 emission filters. Images were acquired using a C9100-13 EM-CCD camera (Hamamatsu, Bridgewater, NJ).

For experiments shown in Figures 5, A–C, and 8 and Supplemental Figure 10, samples were imaged using a Quorum (Guelph, ON, Canada) Discovery TIRF-M, comprising a Leica DMI8 microscope equipped with a 63 $\times$ /1.49 NA TIRF objective with a 1.8 $\times$  camera relay (total magnification 108 $\times$ ). Imaging was done using 488-, 561-, and 637-nm laser illumination and 527/30, 630/75, and 700/75 emission filters and acquired using a Zyla 4.2Plus sCMOS camera (Hamamatsu). For experiments shown in Figure 5, D–F, and Supplemental Figure 5, samples were imaged using the same Quorum Discovery microscope operating in spinning-disk confocal mode.

**CLS detection and quantification of protein fluorescence intensity within CLSs.** CLSs were detected and quantified (Figures 5, 6,

and 8 and Supplemental Figure 11) using custom software developed in Matlab (MathWorks, Natick, MA), as previously described (Aguet et al., 2013; Garay et al., 2015). Briefly, diffraction-limited clathrin structures were detected using a Gaussian-based model method to approximate the point-spread function of eGFP-CLCa, RFP-T-CLCa, or AP2 puncta. The fluorescence intensity corresponding to ligand (A555-EGF, rhodamine-EGF, A555-Tfn, or A647-Tfn) or cytosolic protein (mCh-Sjn1 or endogenous Sjn1) localization within CLSs was determined by the amplitude of the Gaussian model for the appropriate fluorescent channel for each structure. As such, the measurements of fluorescent ligand within CLSs represent enrichment of the corresponding receptors (EGFR or TfR) relative to the local background fluorescence in the vicinity of the detected CLS.

**Measurement of mean fluorescence of ligand or Sjn1 within CLSs.** Measurements of mean A555-EGF (Figure 6C), A555-Tfn (Figure 6E), mCh-Sjn1 (Figure 8B), and endogenous Sjn1 (Supplemental Figure 11) enrichment within CCPs for each cell were subjected to ANOVA followed by Tukey's posttest, with a threshold of  $p < 0.05$  for statistically significant differences between conditions.

**Generation of two-dimensional histogram of EGF and Tfn fluorescence within CLSs.** Measurements of EGF and Tfn fluorescence intensities within CLSs were plotted using a two-dimensional histogram, with 50 bins per channel (Figure 5B). For normalization of differences in EGF and Tfn binding between cells, the fluorescence intensities of EGF or Tfn within CLSs were rescaled by normalization to a value  $n = \mu + 0.75\sigma$ , where  $\mu$  and  $\sigma$  are the mean and SD of the EGF or Tfn intensity within CLSs in each image.

**Identification of EGF- and Tfn-enriched CLSs.** To measure the properties of the subsets of CLSs enriched in fluorescently conjugated EGF or Tfn (and thus the corresponding receptors, EGFR or TfR, respectively; Figures 5, C–F, and 6, D and F), we established a threshold of the ~85th percentile of ligand fluorescence intensity within CLSs in the control (no inhibitor) condition in each experiment (Garay et al., 2015). Note that for the analysis presented in Figure 5, D–G (time course of treatment with EGF and Tfn, images acquired at various z-planes), a common threshold for each experiment was used for all planes and time points within each experiment (corresponding to ventral plane, 3 min of ligand stimulation). Using this threshold, we defined subsets of CLSs enriched in either fluorescent EGF and/or Tfn for each condition as those with ligand fluorescence intensity above this threshold. To validate that this method of sorting CLSs with this arbitrary but systematic threshold effectively produced cohorts of CLSs with the expected enrichment in ligand (and thus receptors), we integrated the ligand signals within each CLS cohort, within each cell, for either TIRF images (Supplemental Figure 4) or spinning-disk confocal images (Supplemental Figure 6). This analysis indicates that the method of delineating CLSs as enriched in specific ligands (e.g., EGF+) effectively produces sorting of CLSs into cohorts based on the presence or absence of specific ligands.

For the experiments in Figure 5, C–F, within each condition, the CLSs were sorted into cohorts that are either positive for only rhodamine-EGF or A647-Tfn or for both. The fraction of CLSs in each cohort (shown as a fraction of CCPs in that specific z-plane for Figure 5, D–F) is reported. For the experiments in Figure 6, D and F, within each condition, the A555-EGF- or A555-Tfn-enriched CLS population was used to measure mean eGFP-CLC fluorescence per CLS in each cell. Measurements (mean eGFP-CLC within the specified CLS subset for each cell) were subjected to ANOVA followed by Tukey's

posttest, with a threshold of  $p < 0.05$  for statistically significant differences between conditions.

### TIRF-M and automated image analysis of CCP properties (time-lapse imaging)

Time-lapse imaging by TIRF-M was performed as previously described (Aguet *et al.*, 2013; Mettlen and Danuser, 2014; Kadlecova *et al.*, 2017). Briefly, RPE cells stably expressing eGFP-CLCa were pretreated with 10  $\mu$ M BAPTA-AM for 15 min (or DMSO vehicle control) and then treated with either 20 ng/ml rhodamine-EGF or 100 ng/ml A647-Tfn (in the presence of 20 ng/ml unlabeled EGF) at the time of imaging. Starting 1 min after ligand addition, time lapse–image series were acquired at a frame rate of 1/s and an exposure time of 80–150 ms using a Quorum Discovery TIRF-M comprising a Leica DMI8 microscope equipped with a 63 $\times$ /1.49 NA TIRF objective with a 1.8 $\times$  camera relay (total magnification 108 $\times$ ). Imaging was done using 488-, 561-, and/or 637-nm laser illumination and 527/30, 630/75, and 700/75 emission filters and acquired using a Zyla 4.2Plus sCMOS camera (Hamamatsu).

The detection, tracking, and analysis of clathrin objects, which allow detection of sCLSs and CCPs, was done as previously described using the cmeAnalysis software package (Aguet *et al.*, 2013; Kadlecova *et al.*, 2017). Briefly, diffraction-limited clathrin structures were detected using a Gaussian-based model method to approximate the point-spread function (Aguet *et al.*, 2013), and trajectories were determined from clathrin-structure detections using u-track software (Jaqaman *et al.*, 2008). sCLSs were distinguished from bona fide CCPs as previously described, based on the quantitative and unbiased analysis of clathrin intensity progression in the early stages of structure formation (Aguet *et al.*, 2013; Kadlecova *et al.*, 2017). Both sCLSs and CCPs represent nucleation events, but only bona fide CCPs represent structures that undergo stabilization, maturation, and in some cases, scission to produce intracellular vesicles (Aguet *et al.*, 2013; Kadlecova *et al.*, 2017). We report the rate of sCLS and CCP formation (Figure 7, C, D, F, and G) and the distribution of CCP lifetimes (Supplemental Figures 8C and 9C), and these measurements were subjected to Student's *t* test, with a threshold of  $p < 0.05$  for statistically significant differences between conditions.

Because CCPs are diffraction-limited objects, the amplitude of the Gaussian model of the fluorescence intensity of eGFP-CLCa indicates CCP size (Figure 7, E and H). In addition, the fluorescence intensity of receptor ligands (rho-EGF or A647-Tfn) indicates the recruitment of the corresponding receptor (Supplemental Figures 8, A and B, and 9, A and B). Given the heterogeneity of CCP lifetimes, for eGFP-CLCa and ligand fluorescence intensity measurements of CCP size and receptor recruitment, objects were separated into lifetime cohorts.

### Whole-cell lysates and Western blotting

Following transfection, serum starvation, and/or treatment with inhibitors as indicated, cells were stimulated with 5 ng/ml EGF for 5 min (unless otherwise indicated) or left unstimulated (basal). Whole-cell lysates were prepared using Laemmli sample buffer (0.5M Tris, pH 6.8, glycerol, 10% SDS, 10%  $\beta$ -mercaptoethanol, and 5% bromophenol blue) supplemented with a protease and phosphatase inhibitor cocktail (1 mM sodium orthovanadate, 10 nM okadaic acid, and 20 nM Protease Inhibitor Cocktail [BioShop, Burlington, ON, Canada]). Lysates were then heated at 65°C for 15 min and passed five times through a 27.5-gauge syringe. Proteins were resolved by glycine-Tris SDS–PAGE followed by transfer onto polyvinylidene fluoride membranes, which were washed, blocked, and incubated with antibodies as previously described (Garay *et al.*, 2015).

The levels of phosphorylated protein in each condition were quantified as previously described (Antonescu *et al.*, 2005). This was done by signal integration in an area corresponding to the appropriate lane and band for each condition. The measurement corresponding to the levels of a phosphorylated form of a specific protein was then normalized to the loading control (e.g., actin) signal and subsequently normalized to the measurement of total protein signal, obtained by a similar method either following blot stripping or reblotting. In each experiment, the resulting normalized phospho/total protein (e.g., phospho-Akt/total Akt) signal in each condition is expressed as a fraction of the normalized pAkt/total Akt measurement in the control condition stimulated with EGF for 5 min. Samples were subjected to ANOVA followed by Tukey's posttest, with a threshold of  $p < 0.05$  for statistically significant differences between conditions (Figure 9 and Supplemental Figure 12).

### ACKNOWLEDGMENTS

We thank Sandra Schmid (University of Texas Southwestern Medical Center) for valuable discussion and feedback and Marcel Mettlen (University of Texas Southwestern Medical Center) for assistance in use of the cmeAnalysis software package. We also thank Anjana Rao for the kind gift of the HA-NFAT1(4-460)-GFP cDNA (Addgene plasmid #11107). Funding for this research was provided by an Operating Grant (no. 125854) and a New Investigator Award from the Canadian Institutes of Health Research, as well as an Early Researcher Award (Ontario Ministry of Research, Innovation and Science) to C.N.A. and an Ontario Graduate Scholarship to R.C.D.S.

### REFERENCES

- Aguet F, Antonescu CN, Mettlen M, Schmid SL, Danuser G (2013). Advances in analysis of low signal-to-noise images link dynamin and AP2 to the functions of an endocytic checkpoint. *Dev Cell* 26, 279–291.
- Alroy I, Yarden Y (1997). The ErbB signaling network in embryogenesis and oncogenesis: signal diversification through combinatorial ligand-receptor interactions. *FEBS Lett* 410, 83–86.
- Antonescu CN, Aguet F, Danuser G, Schmid SL (2011). Phosphatidylinositol-(4,5)-bisphosphate regulates clathrin-coated pit initiation, stabilization, and size. *Mol Biol Cell* 22, 2588–2600.
- Antonescu CN, Danuser G, Schmid SL (2010). Phosphatidic acid plays a regulatory role in clathrin-mediated endocytosis. *Mol Biol Cell* 21, 2944–2952.
- Antonescu CN, Huang C, Niu W, Liu Z, Eyers PA, Heidenreich KA, Bilan PJ, Klip A (2005). Reduction of insulin-stimulated glucose uptake in L6 myotubes by the protein kinase inhibitor SB203580 is independent of p38MAPK activity. *Endocrinology* 146, 3773–3781.
- Antonescu CN, McGraw TE, Klip A (2014). Reciprocal regulation of endocytosis and metabolism. *Cold Spring Harb Perspect Biol* 6, a016964.
- Aramburu J, Yaffe MB, López-Rodríguez C, Cantley LC, Hogan PG, Rao A (1999). Affinity-driven peptide selection of an NFAT inhibitor more selective than cyclosporin A. *Science* 285, 2129–2133.
- Bao J, Alroy I, Waterman H, Schejter ED, Brodie C, Gruenberg J, Yarden Y (2000). Threonine phosphorylation diverts internalized epidermal growth factor receptors from a degradative pathway to the recycling endosome. *J Biol Chem* 275, 26178–26186.
- Bauerfeind R, Takei K, De Camilli P (1997). Amphiphysin I is associated with coated endocytic intermediates and undergoes stimulation-dependent dephosphorylation in nerve terminals. *J Biol Chem* 272, 30984–30992.
- Bone LN, Dayam RM, Lee M, Kono N, Fairn GD, Arai H, Botelho RJ, Antonescu CN (2017). The acyltransferase LYCAT controls specific phosphoinositides and related membrane traffic. *Mol Biol Cell* 28, 161–172.
- Bryant JA, Finn RS, Slamon DJ, Cloughesy TF, Charles AC (2004). EGF activates intracellular and intercellular calcium signaling by distinct pathways in tumor cells. *Cancer Biol Ther* 3, 1243–1249.
- Caldieri G, Barbieri E, Nappo G, Raimondi A, Bonora M, Conte A, Verhoef LGGC, Confalonieri S, Malabarba MG, Bianchi F, *et al.* (2017). Reticulon 3-dependent ER-PM contact sites control EGFR nonclathrin endocytosis. *Science* 356, 617–624.

- Chang CP, Kao JP, Lazar CS, Walsh BJ, Wells A, Wiley HS, Gill GN, Rosenfeld MG (1991). Ligand-induced internalization and increased cell calcium are mediated via distinct structural elements in the carboxyl terminus of the epidermal growth factor receptor. *J Biol Chem* 266, 23467–23470.
- Chen H, Slepnev VI, Di Fiore PP, De Camilli P (1999). The interaction of epsin and Eps15 with the clathrin adaptor AP-2 is inhibited by mitotic phosphorylation and enhanced by stimulation-dependent dephosphorylation in nerve terminals. *J Biol Chem* 274, 3257–3260.
- Choi JH, Park JB, Bae SS, Yun S, Kim HS, Hong WP, Kim IS, Kim JH, Han MY, Ryu SH, et al. (2004). Phospholipase C-gamma1 is a guanine nucleotide exchange factor for dynamin-1 and enhances dynamin-1-dependent epidermal growth factor receptor endocytosis. *J Cell Sci* 117, 3785–3795.
- Conner SD, Schmid SL (2003). Differential requirements for AP-2 in clathrin-mediated endocytosis. *J Cell Biol* 162, 773–779.
- Cornely R, Rentero C, Enrich C, Grewal T, Gaus K (2011). Annexin A6 is an organizer of membrane microdomains to regulate receptor localization and signalling. *IUBMB Life* 63, 1009–1017.
- Cousin MA (2000). Synaptic vesicle endocytosis. *Mol Neurobiol* 22, 115–128.
- Cousin MA, Robinson PJ (2001). The dephosphins: dephosphorylation by calcineurin triggers synaptic vesicle endocytosis. *Trends Neurosci* 24, 659–665.
- Cousin MA, Tan TC, Robinson PJ (2001). Protein phosphorylation is required for endocytosis in nerve terminals: potential role for the dephosphins dynamin I and synaptotagmin, but not AP180 or amphiphysin. *J Neurochem* 76, 105–116.
- Cremona O, Di Paolo G, Wenk MR, Lüthi A, Kim WT, Takei K, Daniell L, Nemoto Y, Shears SB, Flavell RA, et al. (1999). Essential role of phosphoinositide metabolism in synaptic vesicle recycling. *Cell* 99, 179–188.
- Creutz CE, Snyder SL (2005). Interactions of annexins with the mu subunits of the clathrin assembly proteins. *Biochemistry* 44, 13795–13806.
- Delos Santos RC, Garay C, Antonescu CN (2015). Charming neighborhoods on the cell surface: plasma membrane microdomains regulate receptor tyrosine kinase signaling. *Cell Signal* 27, 1963–1976.
- Eichel K, Jullié D, von Zastrow M (2016).  $\beta$ -arrestin drives MAP kinase signaling from clathrin-coated structures after GPCR dissociation. *Nat Cell Biol* 18, 303–310.
- Fu T, Xu Y, Jiang W, Zhang H, Zhu P, Wu J (1994). EGF receptor-mediated intracellular calcium increase in human hepatoma BEL-7404 cells. *Cell Res* 4, 145–153.
- Garay C, Judge G, Lucarelli S, Bautista S, Pandey R, Singh T, Antonescu CN (2015). Epidermal growth factor-stimulated Akt phosphorylation requires clathrin or ErbB2 but not receptor endocytosis. *Mol Biol Cell* 26, 3504–3519.
- Goh LK, Sorkin A (2013). Endocytosis of receptor tyrosine kinases. *Cold Spring Harb Perspect Biol* 5, a017459.
- Grossier J-P, Xouri G, Goud B, Schauer K (2014). Cell adhesion defines the topology of endocytosis and signaling. *EMBO J* 33, 35–45.
- Gual P, Giordano S, Williams TA, Rocchi S, Van Obberghen E, Comoglio PM (2000). Sustained recruitment of phospholipase C-gamma to Gab1 is required for HGF-induced branching tubulogenesis. *Oncogene* 19, 1509–1518.
- Huang F, Khvorova A, Marshall W, Sorkin A (2004). Analysis of clathrin-mediated endocytosis of epidermal growth factor receptor by RNA interference. *J Biol Chem* 279, 16657–16661.
- Irie F, Okuno M, Pasquale EB, Yamaguchi Y (2005). EphrinB-EphB signalling regulates clathrin-mediated endocytosis through tyrosine phosphorylation of synaptotagmin 1. *Nat Cell Biol* 7, 501–509.
- Jaqaman K, Loerke D, Mettlen M, Kuwata H, Grinstein S, Schmid SL, Danuser G (2008). Robust single-particle tracking in live-cell time-lapse sequences. *Nat Methods* 5, 695–702.
- Ji QS, Ermini S, Baulida J, Sun FL, Carpenter G (1998). Epidermal growth factor signaling and mitogenesis in Plcg1 null mouse embryonic fibroblasts. *Mol Biol Cell* 9, 749–757.
- Johannessen LE, Pedersen NM, Pedersen KW, Madhusu IH, Stang E (2006). Activation of the epidermal growth factor (EGF) receptor induces formation of EGF receptor- and Grb2-containing clathrin-coated pits. *Mol Cell Biol* 26, 389–401.
- Jost M, Simpson F, Kavran JM, Lemmon MA, Schmid SL (1998). Phosphatidylinositol-4,5-bisphosphate is required for endocytic coated vesicle formation. *Curr Biol* 8, 1399–1402.
- Kadamur G, Ross EM (2013). Mammalian phospholipase C. *Annu Rev Physiol* 75, 127–154.
- Kadlecova Z, Spielman SJ, Loerke D, Mohanakrishnan A, Reed DK, Schmid SL (2017). Regulation of clathrin-mediated endocytosis by hierarchical allosteric activation of AP2. *J Cell Biol* 216, 167–179.
- Keyel PA, Mishra SK, Roth R, Heuser JE, Watkins SC, Traub LM (2006). A single common portal for clathrin-mediated endocytosis of distinct cargo governed by cargo-selective adaptors. *Mol Biol Cell* 17, 4300–4317.
- Korc M, Matrisian LM, Magun BE (1984). Cytosolic calcium regulates epidermal growth factor endocytosis in rat pancreas and cultured fibroblasts. *Proc Natl Acad Sci USA* 81, 461–465.
- Lamaze C, Baba T, Redelmeier TE, Schmid SL (1993). Recruitment of epidermal growth factor and transferrin receptors into coated pits in vitro: differing biochemical requirements. *Mol Biol Cell* 4, 715–727.
- Lee SY, Wenk MR, Kim Y, Nairn AC, De Camilli P (2004). Regulation of synaptotagmin 1 by cyclin-dependent kinase 5 at synapses. *Proc Natl Acad Sci USA* 101, 546–551.
- Leonard D, Hayakawa A, Lawe D, Lambright D, Bellve KD, Standley C, Lifshitz LM, Fogarty KE, Corvera S (2008). Sorting of EGF and transferrin at the plasma membrane and by cargo-specific signaling to EEA1-enriched endosomes. *J Cell Sci* 121, 3445–3458.
- Liu AP, Aguet F, Danuser G, Schmid SL (2010). Local clustering of transferrin receptors promotes clathrin-coated pit initiation. *J Cell Biol* 191, 1381–1393.
- Liu AP, Loerke D, Schmid SL, Danuser G (2009). Global and local regulation of clathrin-coated pit dynamics detected on patterned substrates. *Biophys J* 97, 1038–1047.
- Liu JP, Sim AT, Robinson PJ (1994). Calcineurin inhibition of dynamin I GTPase activity coupled to nerve terminal depolarization. *Science* 265, 970–973.
- Loerke D, Mettlen M, Schmid SL, Danuser G (2011). Measuring the hierarchy of molecular events during clathrin-mediated endocytosis. *Traffic* 12, 815–825.
- Loerke D, Mettlen M, Yasar D, Jaqaman K, Jaqaman H, Danuser G, Schmid SL (2009). Cargo and dynamin regulate clathrin-coated pit maturation. *PLoS Biol* 7, e57.
- Lucarelli S, Pandey R, Judge G, Antonescu CN (2016). Similar requirement for clathrin in EGF- and HGF-stimulated Akt phosphorylation. *Commun Integr Biol* 9, e1175696.
- MacDonald PE, Eliasson L, Rorsman P (2005). Calcium increases endocytotic vesicle size and accelerates membrane fission in insulin-secreting INS-1 cells. *J Cell Sci* 118, 5911–5920.
- McMahon HT, Boucrot E (2011). Molecular mechanism and physiological functions of clathrin-mediated endocytosis. *Nat Rev Mol Cell Biol* 12, 517–533.
- McPherson PS, Garcia EP, Slepnev VI, David C, Zhang X, Grabs D, Sossin WS, Bauerfeind R, Nemoto Y, De Camilli P (1996). A presynaptic inositol-5-phosphatase. *Nature* 379, 353–357.
- Mettlen M, Danuser G (2014). Imaging and modeling the dynamics of clathrin-mediated endocytosis. *Cold Spring Harb Perspect Biol* 6, a017038.
- Mettlen M, Loerke D, Yasar D, Danuser G, Schmid SL (2010). Cargo- and adaptor-specific mechanisms regulate clathrin-mediated endocytosis. *J Cell Biol* 188, 919–933.
- Mettlen M, Stoerber M, Loerke D, Antonescu CN, Danuser G, Schmid SL (2009). Endocytic accessory proteins are functionally distinguished by their differential effects on the maturation of clathrin-coated pits. *Mol Biol Cell* 20, 3251–3260.
- Miyamoto S, Izumi M, Hori M, Kobayashi M, Ozaki H, Karaki H (2000). Xestospingon C, a selective and membrane-permeable inhibitor of IP(3) receptor, attenuates the positive inotropic effect of alpha-adrenergic stimulation in guinea-pig papillary muscle. *Br J Pharmacol* 130, 650–654.
- Mooibroek MJ, Michiel DF, Wang JH (1987). Clathrin light chains are calcium-binding proteins. *J Biol Chem* 262, 25–28.
- Morris SA, Schmid SL (1995). Synaptic vesicle recycling: the Ferrari of endocytosis? *Curr Biol* 5, 113–115.
- Motley A, Bright NA, Seaman MNJ, Robinson MS (2003). Clathrin-mediated endocytosis in AP-2-depleted cells. *J Cell Biol* 162, 909–918.
- Myers MD, Ryazantsev S, Hicke L, Payne GS (2016). Calmodulin promotes N-BAR domain-mediated membrane constriction and endocytosis. *Dev Cell* 37, 162–173.
- Natke I, Hill B, Parham P, Brodsky F (1990). The calcium-binding site of clathrin light chains. *J Biol Chem* 265, 18621–18627.
- Nunez D, Antonescu C, Mettlen M, Liu A, Schmid SL, Loerke D, Danuser G (2011). Hotspots organize clathrin-mediated endocytosis by efficient recruitment and retention of nucleating resources. *Traffic* 12, 1868–1878.

- Oka T, Sato K, Hori M, Ozaki H, Karaki H (2002). Xestospongine C, a novel blocker of IP3 receptor, attenuates the increase in cytosolic calcium level and degranulation that is induced by antigen in RBL-2H3 mast cells. *Br J Pharmacol* 135, 1959–1966.
- Perera RM, Zoncu R, Lucast L, De Camilli P, Toomre D (2006). Two synaptojanin 1 isoforms are recruited to clathrin-coated pits at different stages. *Proc Natl Acad Sci USA* 103, 19332–19337.
- Puthenveedu MA, von Zastrow M (2006). Cargo regulates clathrin-coated pit dynamics. *Cell* 127, 113–124.
- Ramjaun AR, McPherson PS (1996). Tissue-specific alternative splicing generates two synaptojanin isoforms with differential membrane binding properties. *J Biol Chem* 271, 24856–24861.
- Rappoport JZ, Simon SM (2009). Endocytic trafficking of activated EGFR is AP-2 dependent and occurs through pre-formed clathrin spots. *J Cell Sci* 122, 1301–1305.
- Reis CR, Chen P-H, Bendris N, Schmid SL (2017). TRAIL-death receptor endocytosis and apoptosis are selectively regulated by dynamin-1 activation. *Proc Natl Acad Sci USA* 114, 504–509.
- Reis CR, Chen P-H, Srinivasan S, Aguet F, Mettlen M, Schmid SL (2015). Crosstalk between Akt/GSK3 $\beta$  signaling and dynamin-1 regulates clathrin-mediated endocytosis. *EMBO J* 34, 2132–2146.
- Ross E, Ata R, Thavarajah T, Medvedev S, Bowden P, Marshall JG, Antonescu CN (2015). AMP-activated protein kinase regulates the cell surface proteome and integrin membrane traffic. *PLoS ONE* 10, e0128013.
- Rotin D, Margolis B, Mohammadi M, Daly RJ, Daum G, Li N, Fischer EH, Burgess WH, Ullrich A, Schlessinger J (1992). SH2 domains prevent tyrosine dephosphorylation of the EGF receptor: identification of Tyr992 as the high-affinity binding site for SH2 domains of phospholipase C gamma. *EMBO J* 11, 559–567.
- Saheki Y, De Camilli P (2012). Synaptic vesicle endocytosis. *Cold Spring Harb Perspect Biol* 4, a005645.
- Schmid EM, McMahon HT (2007). Integrating molecular and network biology to decode endocytosis. *Nature* 448, 883–888.
- Schneider CA, Rasband WS, Eliceiri KW (2012). NIH Image to ImageJ: 25 years of image analysis. *Nat Methods* 9, 671–675.
- Sigismund S, Argenzio E, Tosoni D, Cavallaro E, Polo S, Di Fiore PP (2008). Clathrin-mediated internalization is essential for sustained EGFR signaling but dispensable for degradation. *Dev Cell* 15, 209–219.
- Slepnev VI, Ochoa G-C, Butler MH, Grabs D, De Camilli P (1998). Role of phosphorylation in regulation of the assembly of endocytic coat complexes. *Science* 281, 821–824.
- Taylor MJ, Perrais D, Merrifield CJ (2011). A high precision survey of the molecular dynamics of mammalian clathrin-mediated endocytosis. *PLoS Biol* 9, e1000604.
- Tosoni D, Puri C, Confalonieri S, Salcini AE, De Camilli P, Tacchetti C, Di Fiore PP (2005). TTP specifically regulates the internalization of the transferrin receptor. *Cell* 123, 875–888.
- Varnai P, Thyagarajan B, Rohacs T, Balla T (2006). Rapidly inducible changes in phosphatidylinositol 4,5-bisphosphate levels influence multiple regulatory functions of the lipid in intact living cells. *J Cell Biol* 175, 377–382.
- Wijesekara N, Tung A, Thong F, Klip A (2006). Muscle cell depolarization induces a gain in surface GLUT4 via reduced endocytosis independently of AMPK. *Am J Physiol Endocrinol Metab* 290, E1276–E1286.
- Zoncu R, Perera RM, Sebastian R, Nakatsu F, Chen H, Balla T, Ayala G, Toomre D, De Camilli PV (2007). Loss of endocytic clathrin-coated pits upon acute depletion of phosphatidylinositol 4,5-bisphosphate. *Proc Natl Acad Sci USA* 104, 3793–3798.